Thermodynamic Stabilities of Linear and Crinkled Tapes and Cyclic Rosettes in Melamine−Cyanurate Assemblies: A Model Description

Anna G. Bielejewska,[†] **Christopher E. Marjo, Leonard J. Prins, Peter Timmerman,*** **Feike de Jong,*** **and David N. Reinhoudt**

Contribution from the Laboratory of Supramolecular Chemistry and Technology, MESA+ Research Institute, University of Twente, P.O. Box 217, 7500 AE Enschede, The Netherlands

Received March 12, 2001

Abstract: In this paper we describe model calculations for the self-assembly of *N,N*-disubstituted melamines **1** and *N*-substituted cyanuric acid or 5,5-disubstituted barbituric acid derivatives **2** into linear or crinkled tapes and cyclic rosettes via cooperative hydrogen bond formation. The model description considers all possible stereoisomeric tape structures consisting of two to eight different components (270 different species in total) and one cyclic hexameric rosette structure. Furthermore, eight steric parameters (R_{12}−R_{28}) are included that represent the different types of steric interactions within the assemblies. Most importantly, the model calculations clearly show that the tape/rosette ratio is very sensitive to changes in parameters that directly affect the internal energy of the rosette structure. In this respect, three parameters have been characterized, i.e., the basic equilibrium constant K_0 for the bimolecular association of a melamine and cyanurate, the equilibrium constant K_r/K_0 for the cyclization of a linear hexamer, and the parameter R_{12}-a(Z)b, representing attractive or repulsive interactions between adjacent melamine and cyanurate moieties. For example, an increase in K_0 from 100 to 10 000 M^{-1} ($[A]_0 = [B]_0 = 10$ mM, $K_r = 0.01$ M) or in K_r from 0.001 to 0.1 M ($[A]_0 = [B]_0 = 10$ mM, $K_0 = 1000$ M^{-1}) raises the concentration of the rosette from <5 to ∼90% or from ∼10 to ∼85%, respectively. Similarly, a change in R_{12}-a(Z)b from 1.0 (no repulsive or attractive interactions) to 1.5 (slight attractive interaction) raises the rosette fraction of the mixture from 25% to 45%. In sharp contrast to this, the model calculations show that parameters that only affect the internal energy of the tapes (R_{13}−R_{28}) hardly change the tape/rosette ratio. For example, by changing R_{13}-a(*EE*)a from 1.0 (no repulsive or attractive interactions) to 0.001 (maximum repulsion), the rosette fraction in the mixture changes by *no more than 8%.* Including all possible sterics that occur only in tapes (i.e., R_{13}−R_{28}), the maximum change in rosette fraction is no more than 16%. These predictions can be rationalized by considering that any change in the stability of the tapes only affects the rosette concentration by means of shifting the equilibrium between free **1** and **2** and the rosette. Since there are 270 different tapelike structures in equilibrium, *this mixture represents the best buffer solution in the world.* These model calculations seem to conflict with the concept of peripheral crowding as put forward by Whitesides et al., which states that bulky substituents on the periphery of the melamine (and cyanurate) components can be used to shift the tape/rosette equilibrium completely toward the rosette structure. Computer simulations (CHARMm 24.0) show that linear tapes with bulky substituents are severely distorted from planarity, while the corresponding rosette remains planar. Therefore, tapelike structures with bulky substituents are expected to have a much higher solubility than the corresponding rosettes, which can explain the observed crystal data.

Introduction

The formation of reversible polymeric structures using hydrogen-bonding interactions has been an active topic of research during the past decade.[1−9] More than 30 years ago, the first X-ray crystal data on polymeric hydrogen-bonded arrays based on isophthalic and trimesic acid were reported.[10,11] These findings have initiated the structural design of similar hydrogen-bonded networks, both in the solid state[12−17] and in solution.[18−21]

* To whom correspondence should be addressed. E-mail: p.timmerman@ct.utwente.nl.

† Present address: Institute of Physical Chemistry, Polish Academy of Sciences Kasprzaka 44/53, 01-224 Warsaw, Poland.

(1) Fouquey, C.; Lehn, J.-M.; Levelut, A.-M. *Adv. Mater.* **1990,** *2,* 254−257.

(2) Garcia-Tellado, F.; Geib, S. J.; Goswami, S.; Hamilton, A. D. *J. Am. Chem. Soc.* **1991,** *113,* 9265−9269.

(3) Geib, S. J.; Vincent, C.; Fan, E.; Hamilton, A. D. *Angew. Chem.* **1993,** *105,* 83−85; *Angew. Chem., Int. Ed. Engl.* **1993,** *32,* 119−121.

(4) Kotera, M.; Lehn, J.-M.; Vigneron, J.-P. *J. Chem. Soc., Chem. Commun.* **1994,** 197−199.

(5) Sijbesma, R. P.; Beijer, F. H.; Brunsveld, L.; Folmer, B. J. B.; Hirschberg, J. H. K. K.; Lange, R. F. M.; Lowe, J. K. L.; Meijer, E. W. *Science* **1997,** *278,* 1601−1604.

(6) Castellano, R. K.; Rudkevich, D. M.; Rebek, J., Jr. *Proc. Natl. Acad. Sci. U.S.A.* **1997,** *94,* 7132−7137.

(7) Lange, R. F. M.; Van Gurp, M.; Meijer, E. W. *J. Polym. Sci., Part A: Polym. Chem.* **1999,** *37,* 3657−3670.

(8) Würthner, F.; Thalacker, C.; Sautter, A. *Adv. Mater.* **1999,** *11,* 754−758.

(9) Würthner, F.; Thalacker, C.; Sautter, A.; Schaertl, W.; Ibach, W.; Hollricher, O. *Chem. Eur. J.* **2000,** *6,* 3871−3886.

(10) Duchamp, D. J.; Marsh, R. E. *Acta Crystallogr., Sect. B: Struct. Sci.* **1969,** *25,* 5−19.

(11) Alcala, R.; Martinez-Carrera, S. *Acta Crystallogr., Sect. B: Struct. Sci.* **1972,** *28,* 1671−1677.

(12) Zerkowski, J. A.; Seto, C. T.; Wierda, D. A.; Whitesides, G. M. *J. Am. Chem. Soc.* **1990,** *112,* 9025−9026.

(13) Lehn, J.-M.; Mascal, M.; DeCian, A.; Fischer, J. *J. Chem. Soc., Chem. Commun.* **1990,** 479−480.

(14) Kolotuchin, S. V.; Fenlon, E. E.; Wilson, S. R.; Loweth, C. J.; Zimmerman, S. C. *Angew. Chem.* **1995,** *107,* 2873−2876; *Angew. Chem., Int. Ed. Engl.* **1995,** *34,* 2654−2657.
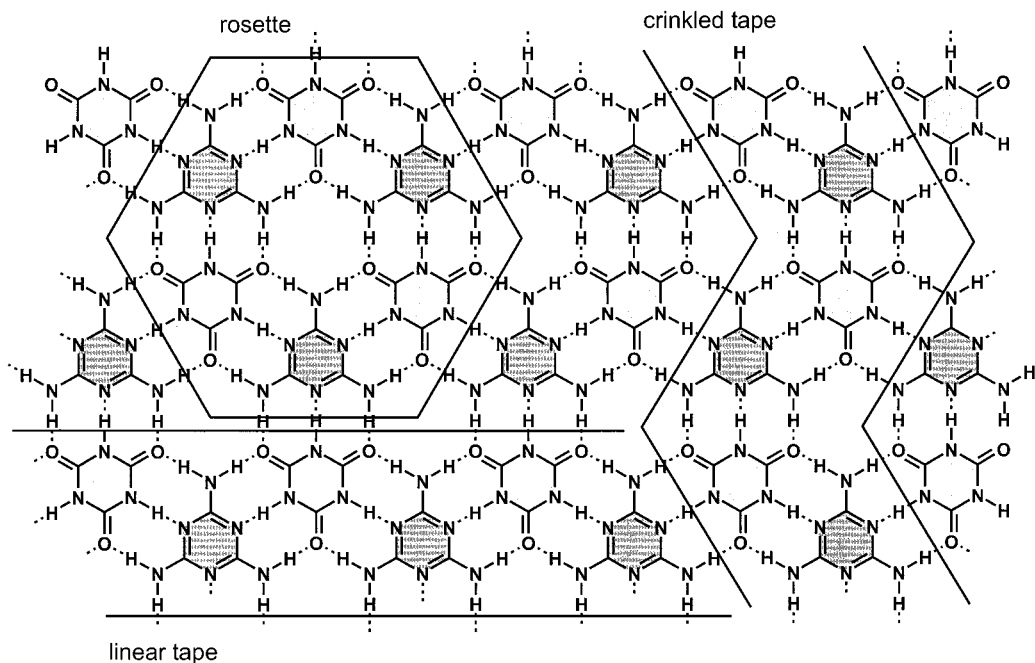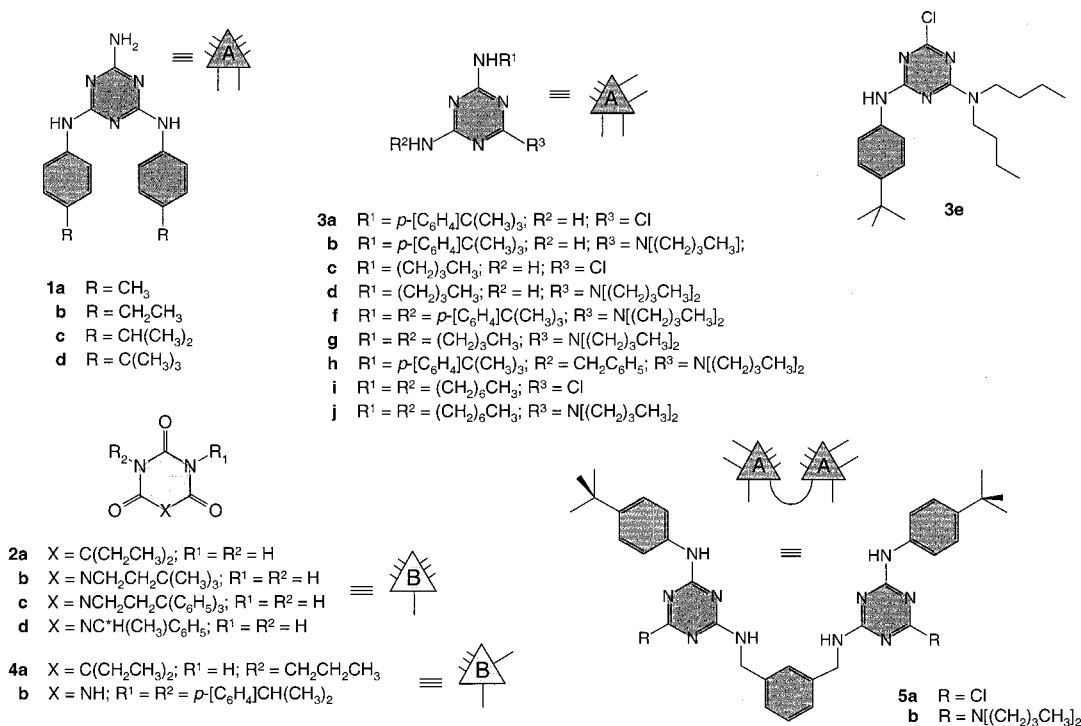
Figure 1. Schematic representation of the cyanuric acid−melamine (CA·M) lattice. Gray-shaded regions represent three different types of substructures in the lattice, i.e., the linear tape, the crinkled tape, and the cyclic rosette.

Chart 1

Complementary hydrogen bond formation between cyanuric acid (CA) and melamine (M) in the CA·M lattice (Figure 1) is among the most well-studied structural motifs for self-assembly of linear and cyclic hydrogen-bonded assemblies.[22,23] The hydrogen-bond-directed assembly of melamine and cyanurate derivatives **1** and **2** (Chart 1) can, in principle, give rise to the formation of three different types of aggregates, viz. the (finite) cyclic *rosettes*, the (infinite) *linear tapes*, or the (infinite) *crinkled tapes* (Figure 1). For most assemblies, solution-phase studies are severely hampered by rapid exchange of components

(15) Mascal, M.; Fallon, P. S.; Batsanov, A. S.; Heywood, B. R.; Champ, S.; Colclough, M. *J. Chem. Soc., Chem. Commun.* **1995**, 805−806.

(16) Zafar, A.; Yang, J.; Geib, S. J.; Hamilton, A. D. *Tetrahedron Lett.* **1996**, *37*, 2327−2330.

(17) Valiyaveettil, S.; Müllen, K. *New J. Chem.* **1998**, 89−95.

(18) Seto, C. T.; Whitesides, G. M. *J. Am. Chem. Soc.* **1990**, *112*, 6409−6411.

(19) Wyler, R.; De Mendoza, J.; Rebek, J., Jr. *Angew. Chem.* **1993**, *105*, 1820−1822; *Angew. Chem., Int. Ed. Engl.* **1993**, *32*, 1699−1701.

(20) Yang, J.; Marendaz, J.-L.; Geib, S. J.; Hamilton, A. D. *Tetrahedron Lett.* **1994**, *35*, 3665−3668.

(21) Zeng, F.; Zimmerman, S. C. *Chem. Rev.* **1997**, *97*, 1681−1712.

(22) Ranganathan, A.; Pedireddi, V. R.; Rao, C. N. R. *J. Am. Chem. Soc.* **1999**, *121*, 1752−1753.

(23) Whitesides, G. M.; Simanek, E. E.; Mathias, J. P.; Seto, C. T.; Chin, D. N.; Mammen, M.; Gordon, D. M. *Acc. Chem. Res.* **1995**, *28*, 37−44.

between rosettes and tapelike structures, which precludes an accurate estimation of the rosette/tape ratio, e.g., by ^{1}H NMR spectroscopy. Therefore, most solution-phase studies deal with rosette structures for which the thermodynamic stability has been increased by means of covalent Hub spacers (*covalent pre-organization*).[18,24,25] In addition to this, the solubility of tapelike assemblies is usually very low in apolar solvents, like chloroform and toluene. For this reason, most structural information comes from X-ray crystal diffraction studies with a wide variety of different 1:1 CA·M complexes.[12,26-28] These studies show the formation of *linear* tapes for melamines with sterically nondemanding substituents, like para-substituted phenyl groups or *m*-fluorophenyl, *m*-methylphenyl, or *m*-iodophenyl groups,[28] while *crinkled* tapes are formed for melamines with sterically bulkier groups, like *tert*-butyl,[27] *p*-(methoxycarbonyl)phenyl,[26] or *m*-chlorophenyl or *m*-bromophenyl substituents.[28] Only for melamine **1d**, carrying the bulkiest 4-(*tert*-butyl)phenyl side group was the cyclic rosette structure observed in the solid state.[26,29] Related X-ray studies on other H-bonded systems show very different results. For example, Hamilton's group showed that 5-decyloxyisophthalic acid forms a cyclic hexamer in the solid state, while there is no apparent influence of steric interactions.[20] Moreover, Valiyaveettil and Müllen showed that 5-alkoxy-substituted isophthalic acids preferentially crystallize as cyclic hexamers for alkyl chain lengths of 6−10 C atoms, while for the longer alkyl chains (>12 C-atoms) the linear tapelike structures are observed in the solid state.[17] These apparently contradictory X-ray data clearly emphasize the total lack of understanding of the self-assembly process of this type of hydrogen-bond-directed aggregates. For a useful application of these polymeric structures, one should be able to identify the structural parameters that drive the assembly toward one particular type of aggregate.

In the course of our investigations on the self-assembly of calix[4]arene double rosette assemblies,[30-39] we became interested in a fundamental understanding of the process of tape vs

(24) Seto, C. T.; Whitesides, G. M. *J. Am. Chem. Soc.* **1991**, *113*, 712−713.

(25) Mathias, J. P.; Simanek, E. E.; Seto, C. T.; Whitesides, G. M. *Angew. Chem.* **1993**, *105*, 1848−1852; *Angew. Chem., Int. Ed. Engl.* **1993**, *32*, 1766−1769.

(26) Zerkowski, J. A.; Seto, C. T.; Whitesides, G. M. *J. Am. Chem. Soc.* **1992**, *114*, 5473−5475.

(27) Zerkowski, J. A.; Whitesides, G. M. *J. Am. Chem. Soc.* **1994**, *116*, 4298−4304.

(28) Zerkowski, J. A.; Mathias, J. P.; Whitesides, G. M. *J. Am. Chem. Soc.* **1994**, *116*, 4305−4315.

(29) Mathias, J. P.; Simanek, E. E.; Zerkowski, J. A.; Seto, C. T.; Whitesides, G. M. *J. Am. Chem. Soc.* **1994**, *116*, 4316−4325.

(30) Vreekamp, R. H.; Van Duynhoven, J. P. M.; Hubert, M.; Verboom, W.; Reinhoudt, D. N. *Angew. Chem.* **1996**, *108*, 1306−1309; *Angew. Chem., Int. Ed. Engl.* **1996**, *35*, 1215−1218.

(31) Timmerman, P.; Vreekamp, R. H.; Hulst, R.; Verboom, W.; Reinhoudt, D. N.; Rissanen, K.; Udachin, K. A.; Ripmeester, J. *Chem. Eur. J.* **1997**, *3*, 1823−1832.

(32) Crego Calama, M.; Hulst, R.; Fokkens, R.; Nibbering, N. M. M.; Timmerman, P.; Reinhoudt, D. N. *Chem. Commun.* **1998**, 1021−1022.

(33) Jolliffe, K. A.; Crego Calama, M.; Fokkens, R.; Nibbering, N. M. M.; Timmerman, P.; Reinhoudt, D. N. *Angew. Chem.* **1998**, *110*, 1294−1297; *Angew. Chem., Int. Ed. Engl.* **1998**, *37*, 1247−1251.

(34) Prins, L. J.; Huskens, J.; De Jong, F.; Timmerman, P.; Reinhoudt, D. N. *Nature (London)* **1999**, *398*, 498−502.

(35) Prins, L. J.; Jolliffe, K. A.; Hulst, R.; Timmerman, P.; Reinhoudt, D. N. *J. Am. Chem. Soc.* **2000**, *122*, 3617−3627.

(36) Prins, L. J.; De Jong, F.; Timmerman, P.; Reinhoudt, D. N. *Nature* **2000**, *408*, 181−184.

(37) Cardullo, F.; Crego Calama, M.; Snellink-Ruel, B. H. M.; Weidmann, J.-L.; Bielejewska, A.; Fokkens, R.; Nibbering, N. M. M.; Timmerman, P.; Reinhoudt, D. N. *Chem. Commun.* **2000**, 367−368.

(38) Timmerman, P.; Jolliffe, K. A.; Crego Calama, M.; Weidmann, J.-L.; Prins, L. J.; Cardullo, F.; Snellink-Ruel, B. H. M.; Fokkens, R.; Nibbering, N. M. M.; Shinkai, S.; Reinhoudt, D. N. *Chem. Eur. J.* **2000**, *6*, 4104−4115.
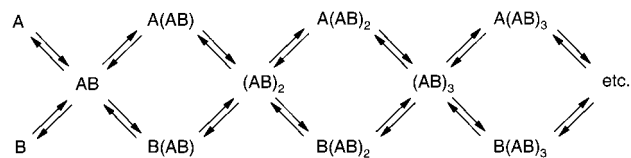
Figure 2. Formation of $(AB)_n$, $A(AB)_n$, and $B(AB)_n$ oligomers via complementary hydrogen-bonding between components A and B.

rosette formation in single CA·M assemblies, and of the thermodynamic parameters that determine their relative stabilities. In this paper we describe a theoretical model that was developed in our group for the calculation of the fraction of linear (tapes) and cyclic (rosettes) assemblies in an equilibrating mixture of bifunctional components ⟨A⟩ and ⟩B⟨. The calculations clearly show that the assembly process is primarily characterized by the K_0 and K_r values (for definitions, see eqs 1 and 7−9) and that steric interactions play only a minor role in the process. Therefore, earlier conclusions (peripheral crowding concept) need to be reevaluated.

Model Descriptions

In this paper we describe model calculations using two different models. The first model is a purely statistical model that considers an infinite number of linear species that are in equilibrium with one cyclic species. This model neglects any type of stereoisomerism or steric interactions within the assemblies. The second model considers only a limited number of assemblies, i.e., one cyclic rosette structure and all tapelike structures consisting of 2−8 components, including all possible stereoisomers (271 species in total). Additionally, this model takes into account all steric interactions (36 different types) that can possibly occur between the side chains of components ⟨A⟩ and ⟩B⟨. Using experimentally determined binding constants for crippled melamines **3** and cyanurate or barbiturate derivatives **4** as input (vide infra), we studied how both thermodynamic (K_0 and K_r) and steric parameters (R_{12}−R_{28}) affect the ratio of tapelike and rosette structures in solution.

Formally speaking, we only need model 1 to prove that the simplification of model 2 (only 270 instead of an infinite number of tapes) is allowed. When the conditions (K_0, K_r, A_0, B_0) are such that model 1 predicts all mass (say, >98%) to be located in the first eight generations of assemblies (up to ⟨(AB)$_4$⟨), we feel safe to use the simplified model 2.

Model 1: Statistical Model of Self-Assembly. The basic rules for self-assembly leading to linear and cyclic oligomers were recently discussed in an excellent paper by Ercolani,[40] who presented a quantitative description of the self-assembly process. In the present paper we follow a similar approach to describe rosette formation (Figure 2).

First, we define K_0 as the association constant for the binding between two monofunctional (crippled) units |A⟩ and |B⟨:

$$|A\rangle + |B\langle \overset{K_0}{\rightleftharpoons} |A\rangle\rangle B| \qquad (1)$$
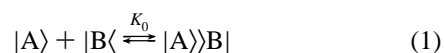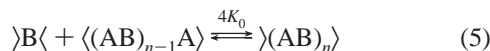
In this way, association of bifunctional partners (⟨A⟩ and ⟩B⟨) will lead to a value of $4K_0$, where the number 4 accounts for the four different modes of association. The self-assembly of two bifunctional complementary monomers ⟨A⟩ and ⟩B⟨ can be described by a process in which oligomerization (tape formation) competes with cyclization (rosette formation). The former

(39) Timmerman, P.; Weidmann, J.-L.; Jolliffe, K. A.; Prins, L. J.; Reinhoudt, D. N.; Shinkai, S.; Frish, L.; Cohen, Y. *J. Chem. Soc., Perkin Trans. 2* **2000**, *10*, 2077−2089.

(40) Ercolani, G. *J. Phys. Chem. B* **1998**, *102*, 5699−5703.

process leads to three subtypes of tapes, namely $\langle(AB)_nA\rangle$, $\rangle B(AB)_n\langle$, and $\langle(AB)_n\langle$, and under equilibrium conditions the following relations will hold:

$$\langle A\rangle + \rangle B(AB)_{n-1}A\rangle \overset{K_0}{\rightleftharpoons} \langle(AB)_nA\rangle \qquad (2)$$

$$\rangle B\langle + \rangle B(AB)_{n-1}A\rangle \overset{K_0}{\rightleftharpoons} \rangle B(AB)_n\langle \qquad (3)$$

$$\langle A\rangle + \rangle B(AB)_{n-1}\langle \overset{4K_0}{\rightleftharpoons} \langle(AB)_n\langle \qquad (4)$$

$$\rangle B\langle + \langle(AB)_{n-1}A\rangle \overset{4K_0}{\rightleftharpoons} \rangle(AB)_n\rangle \qquad (5)$$
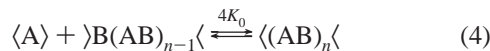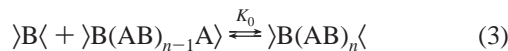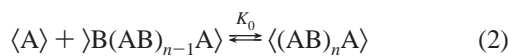
Assuming that the geometrical positioning of the functionality in monomers $\langle A\rangle$ and $\rangle B\langle$ is such that they can only form one specific cycle R_r, its formation can be described in three different ways.

First, the formation of the cycle R_r can be envisaged from its open precursor ($n = r$) through cyclization:

$$\langle(AB)_r\langle \overset{K_c}{\rightleftharpoons} R_r \qquad (6)$$

The "cyclization constant" K_c can be related to K_0 through $K_c = K_r K_0$, where K_r is the "effective molarity".[41] The constant K_r also relates to the equilibria in which the cycle is formed from large ($n > r$) oligomers in each string by a back-biting process:

$$\langle(AB)_nA\rangle \overset{K_r}{\rightleftharpoons} R_r + \langle(AB)_{n-r}A\rangle \qquad (7)$$

$$\rangle B(AB)_n\langle \overset{K_r}{\rightleftharpoons} R_r + \rangle B(AB)_{n-r}\langle \qquad (8)$$

$$\langle(AB)_n\langle \overset{K_r}{\rightleftharpoons} R_r + \langle(AB)_{n-r}\langle \qquad (9)$$

In this approach, K_r resembles the "molar cyclization equilibrium constant" originally introduced by Jacobson and Stockmayer in their fundamental treatment of cyclization processes.[42]

Furthermore, the formation of R_r can also occur through the combination of two smaller oligomers:

$$\langle(AB)_iA\rangle + \rangle B(AB)_{r-i-1}\langle \overset{4K_0}{\rightleftharpoons} \langle(AB)_r\langle \qquad (10)$$
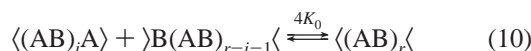
This relation follows directly from a combination of eqs 4−6, leading to the following expression for K_{plug}:

$$\langle(AB)_iA\rangle + \rangle B(AB)_{r-i-1}\langle \overset{K_{plug}}{\rightleftharpoons} R_r \qquad (11)$$
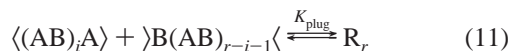
where $K_{plug} = 4K_0^2 K_r$.

Finally, we can describe the formation of R_r also from its basic components A and B:

$$r\langle A\rangle + r\rangle B\langle \overset{K_{ag}}{\rightleftharpoons} R_r \qquad (12)$$

with $$K_{ag} = K_r(4K_0^2)^r \qquad (13)$$

Given an expression Q:

$$Q = (4K_0^2)[A][B] \qquad (14)$$

the mass balances for A and B become

(41) Mandolini, L. *Adv. Phys. Org. Chem.* **1986**, *22*, 1−111.
(42) Jacobson, H.; Stockmayer, W. H. *J. Chem. Phys.* **1950**, *18*, 1600−1612.

$$A_0 = [A]/(1 - Q) + ([A] + [B] + 1/K_0)Q/ (1 - Q)^2 + rK_rQ^r \qquad (15)$$

$$B_0 = [B]/(1 - Q) + ([A] + [B] + 1/K_0)Q/ (1 - Q)^2 + rK_rQ^r \qquad (16)$$

Hence, when K_0 and K_r are known, the concentration of free monomer A and B can be calculated from eqs 14 and 15 by numerical methods using the Solver in Excell, and the concentrations of the self-assembled species follow from

$$[\langle(AB)_n\langle] = Q^n/K_0 \qquad (17)$$

$$[\langle(AB)_nA\rangle] = [A]Q^n \qquad (18)$$

$$[\rangle B(AB)_n\langle] = [B]Q^n \qquad (19)$$

$$[R_r] = K_rQ^r \qquad (20)$$

Model 2: Self-Assembly Including Steric Interactions. The topology of the agglomeration process is shown schematically in Figure 3. When A and B have two identical binding sites (a and b respectively), and sites a and b are complementary and A and B do not self-assemble, each bond formation between A and B can occur in two stereochemically different ways, E and Z, respectively (Figure 4).

When i molecules of A and j molecules of B are allowed to form an assembly A_iB_j through the formation of $i + j - 1$ bonds (the stoichiometry requires that $j = i$, or $j = i\pm1$), the number of possible isomers (N) is given by

$$N (i = j) = 2^{i+j-1} \qquad (21)$$

$$N (i \neq j) = 2^{i+j-1} + 2^{(i+j-1)/2} \qquad (22)$$

Each isomer A_iB_j is now characterized by (i) the number of A units, i; (ii) the number of B units, j; (iii) a probability factor P (1 for symmetric, 2 for asymmetric molecules); and (iv) the steric arrangement of each of the $i + j - 1$ bonds in terms of E or Z.

When we define the real association constant for the formation of a particular bond between fragments A and B as K_{real}, we can define a repulsion factor for the formation of this bond as $R_{pq} = K_{real}/K_0$, K_0 being the association constant for the unrestricted bond formation (vide supra).

This leads to the following expression for the concentration of isomer A_iB_j:

$$[A_iB_j] = PK_0(i + j - 1)A^iB^j(\Pi R_{pq}) \qquad (23)$$

where the summation is over all its $i + j - 1$ bonds.

Rosette (R) formation is thought to occur by ring-closure of the "pre-rosette" molecule A_3B_3 with the proper *all-Z* stereochemistry:

$$[\langle(AB)_3\langle]_{ZZZZZ} \overset{K_{cs}}{\rightleftharpoons} R_r \qquad (24)$$
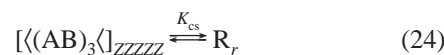
The equilibrium constant K_{cs} is related to the cyclization constant K_c in the statistical model (model 1) through

$$K_{cs} = 32K_c \qquad (25)$$

since only 1 out of 2^5 isomers has the proper geometry for cyclization.
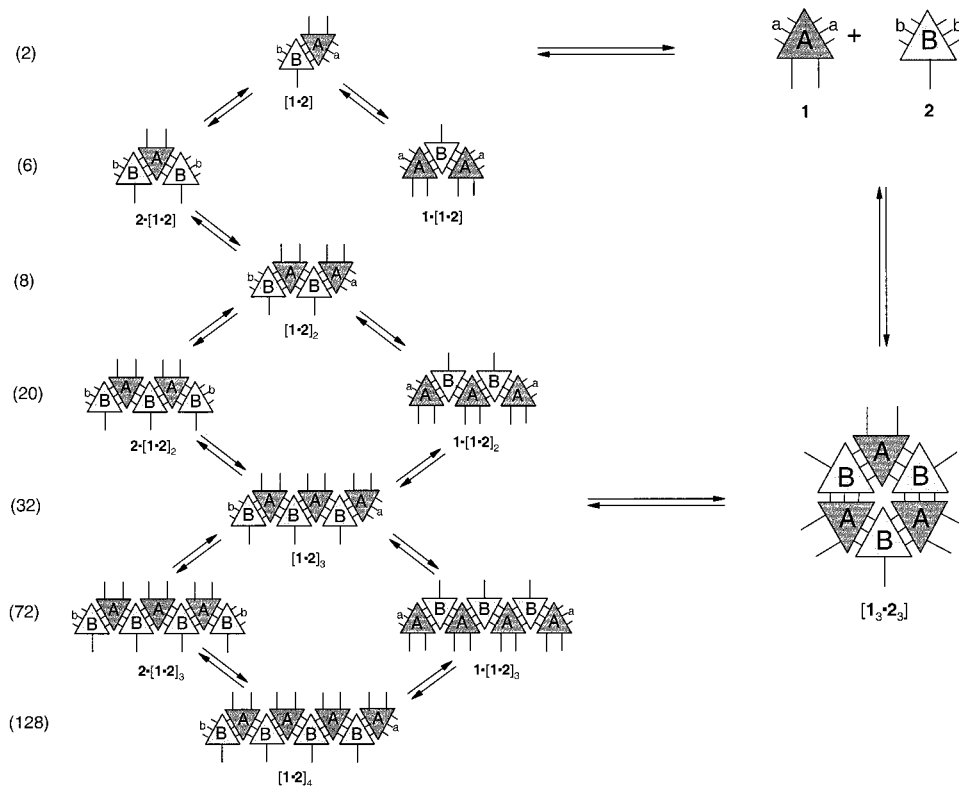
Figure 3. Schematic representation of the various different hydrogen-bonded assemblies present in a dynamic mixture of components **1** and **2** (numbers on the left represent the number of different stereoisomers that were considered in the model calculations).
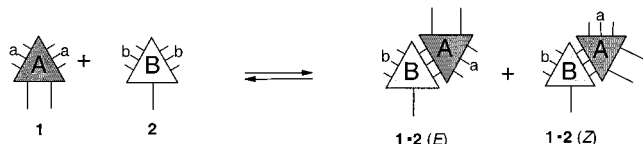

Figure 4. Schematic representation of the *E* ("entgegen") and *Z* ("zusammen") orientation of components **1** (A) and **2** (B).

From eqs 23 and 25 and the mass balances for A and B (eqs 26 and 27), the system can, in principle, be solved by numerical methods, once proper estimates for the repulsion factors have been made.

$$A_0 = \sum_i A_i B_j + 3R \qquad (26)$$

$$B_0 = \sum_i A_i B_j + 3R \qquad (27)$$

Model Calculations

The models described above have been implemented in MicroMath Scientist 2.01 or Microsoft Excel 97 (for details, see Experimental Section) for a system consisting of free melamine **1** and cyanurate **2** in equilibrium with a large collection (270 different species) of linear and crinkled tapes and one single rosette structure ($1_3 \cdot 2_3$, see Figure 3). The second model takes into account all possible stereoisomers of tapelike assemblies up to $[1 \cdot 2]_4$. The whole assembly process can be described by just two equilibrium constants: the basic association constant K_0 and the equilibrium constant K_r, specifying rosette formation. Moreover, a total of 36 steric repulsion factors were included (see Figure 5) in order to account for all possible steric interactions that can be present in either tapes and/or rosette according to modeling studies.

The composition of the mixture can be calculated as a function of equilibrium constants K_0 and K_r and the initial total concentrations of **1** and **2**. These calculations are performed using a steric factor $R_{pq} = 1$ ($K_{real} = K_0$), which means that we do not consider any of the steric effects (no repulsion or attraction) at this point. These calculations show the following results.

There is an optimal concentration for rosette formation, as illustrated in Figure 6. At infinite dilution, the assemblies are completely dissociated, and only free **1** and **2** are present. Upon increasing the concentration $[\mathbf{1}]_0$ (and also $[\mathbf{2}]_0$), the rosette $1_3 \cdot 2_3$ starts to form until a maximum value of K_r at infinite concentration. However, the fraction of **1** present in the rosette goes through a maximum, the position of which follows directly from the model ($[\mathbf{1}]_{max} = x/(1 + x)$, where $x = 24K_0K_r$ ($5^5/7^7$). Above this value, the rosette fraction decreases in favor of tapelike structures, the concentration of which further increases upon increasing the concentration. The concentration of free **1** reaches a maximum value of $1/(2K_0)$ at infinite concentration, whereas the fraction of free **1** goes to zero at infinite concentration. In contrast to what Hunter suggested in an earlier paper, we do not favor the definition of a "critical self-assembly concentration (csac)",[43] since we observe only a maximum in the fraction of free **1** and/or **2** and rosette. Calculations in which the ratio of **1/2** is varied (see Figure 7) clearly reveal a maximum in the rosette fraction for equimolar mixtures of **1** and **2**.

The fraction of rosette depends strongly on the value of K_0. For example, at fixed values of K_r (0.01 M), [**1**], and [**2**] (both 10 mM), an increase in K_0 from 100 to 10 000 M^{-1} changes the fraction of rosette from <5% to ~90% at the expense of both free **1** and **2** and the tapes (see Figure 8A). Similarly, the fraction of rosette is changed dramatically with variations in the value of K_r. For fixed values of K_0 (1000 M^{-1}) and [**1**] and

(43) Xianglan, C.; Guerin, A. J.; Haycock, R. A.; Hunter, C. A.; Sarson, L. A. *J. Chem. Soc., Chem. Commun.* **1995**, 2563−2565.
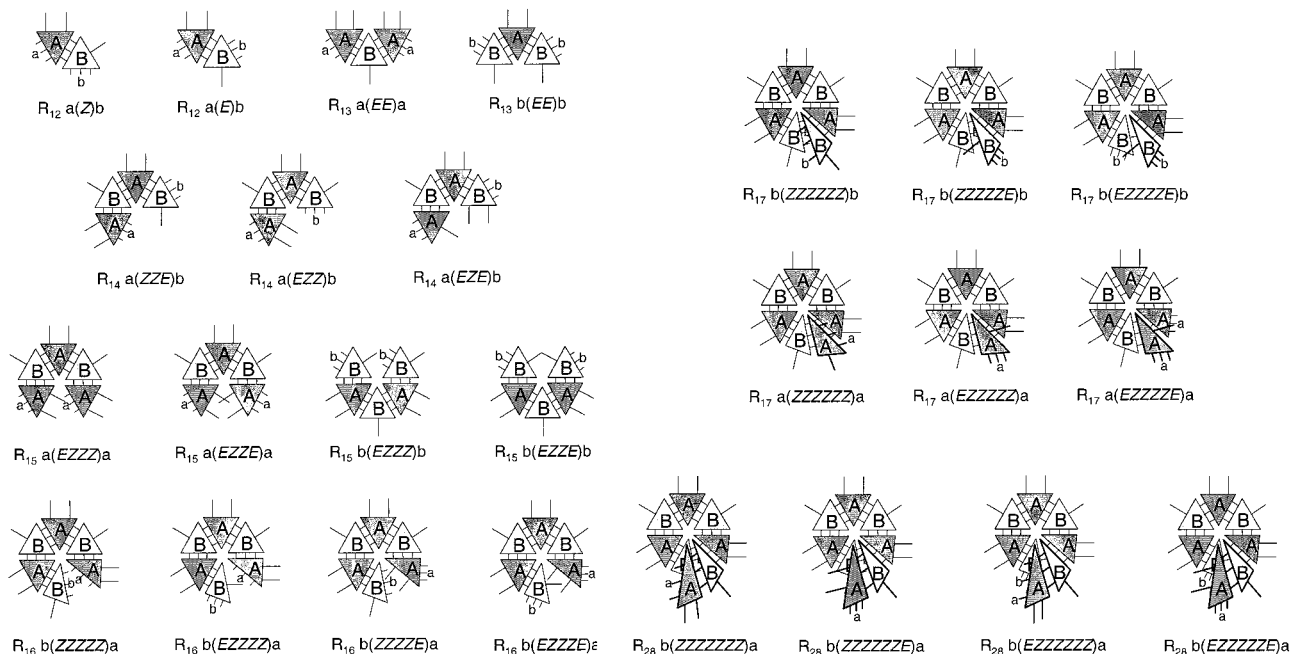
Figure 5. Illustration of the 36 different types of steric interactions (R$_{12}$−R$_{28}$) that are considered in the model calculations.
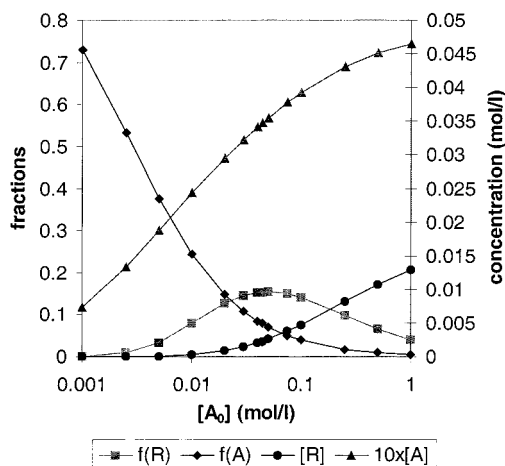

Figure 6. Variation in the composition of an equilibrating mixture of free A, free B, tapes [AB]$_n$, A[AB]$_n$, B[AB]$_n$, and rosette A$_3$·B$_3$ as a function of [A]$_0$ (=[B]$_0$). Conditions: $K_0 = 100$ M^{-1}, $K_r = 0.02$. (N.B.: no steric repulsions are included in these calculations.)

Figure 7. Fraction of rosette in an equilibrating mixture of free A and B as a function of [A]$_0$. Conditions: [A]$_0$ + [B]$_0$ = 25.8 mM, K_0 = 400 M^{-1}, $K_r = 0.005$ M.

[**2**] (both 10 mM), the fraction of rosette increases from 10 to 85% at the expense of tapelike structures upon increasing K_r from 0.001 to 0.1 M (see Figure 8B). The changes in rosette fraction as a function of both K_0 and K_r are represented in the 2D plot given in Figure 9.

It is interesting to note that the fraction of tapes reaches a maximum of 70% around $K_0 \approx 500$ M^{-1}, while it then rapidly decreases upon further increasing the value of K_0 (<10% at K_0 > 10 000 M^{-1}, see Figure 8A). These impressive changes in the rosette fraction as a function of both K_0 and K_r are understandable considering the fact that both parameters directly influence the internal energy (E_{int}) of the rosette. Later we will see that parameters that influence the rosette fraction in an indirect manner (e.g., R$_{13}$ a(*EE*)a) have a much smaller effect on the composition of the mixture.

Subsequently, the influence of steric parameters on the composition of the assembly process was studied. As mentioned earlier, a total of 36 different steric parameters (R$_{12}$−R$_{28}$) was included in the model that represent all the possible steric interactions that can be present in the assemblies according to
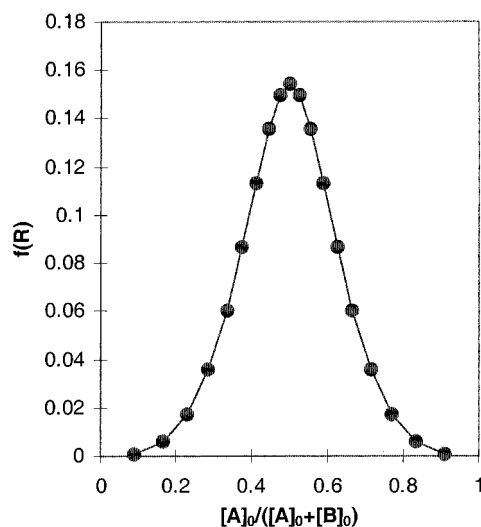
molecular modeling studies (see Figure 5). Each parameter was gradually decreased from 1 to 0.001 in order to mimic repulsion, or from 1 to 2 in order to mimic attraction, and the corresponding rosette fractions in the mixture were calculated (see Figures 10 and 11). These results clearly show that the rosette fraction is extremely sensitive to steric repulsion in the R$_{12}$-a(*Z*)b fashion (see Figure 5). A reduction of R$_{12}$-a(*Z*)b from 1 (no repulsion) to 0.5 (slight repulsion) reduces the rosette fraction from 25% to <5%. On the other hand, when this interaction is made slightly attractive (from 1 to 1.5), the rosette fraction increases to 45%.

Surprisingly, the effect of steric interactions in the R$_{13}$-a(*EE*)a fashion (see Figure 5) in linear tapes, which has so far been regarded as the most important parameter to direct rosette formation,[20,26,29,44] is only very modest. For example, a decrease in R$_{13}$-a(*EE*)a from 1 (no repulsion) to 0.001 (extremely strong

(44) Mathias, J. P.; Simanek, E. E.; Whitesides, G. M. *J. Am. Chem. Soc.* **1994**, *116*, 4326−4340.
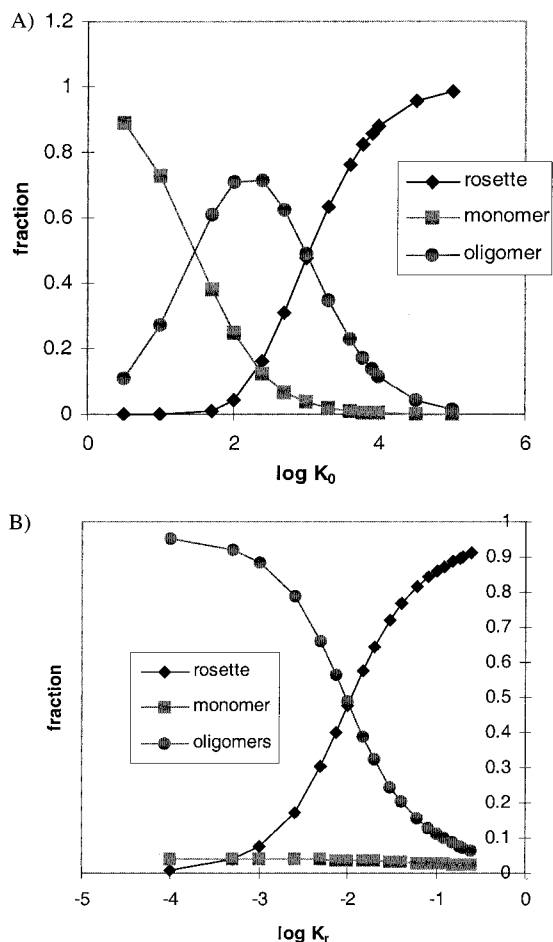
Figure 8. Effect of (A) K_0 ($r = 3$, $A_0 = B_0 = 10$ mM, $K_r = 0.01$ M) and (B) K_r ($r = 3$, $A_0 = B_0 = 10$ mM, $K_0 = 1000$ M^{-1}) on the composition of a dynamic mixture of hydrogen-bonded melamine—cyanurate assemblies.
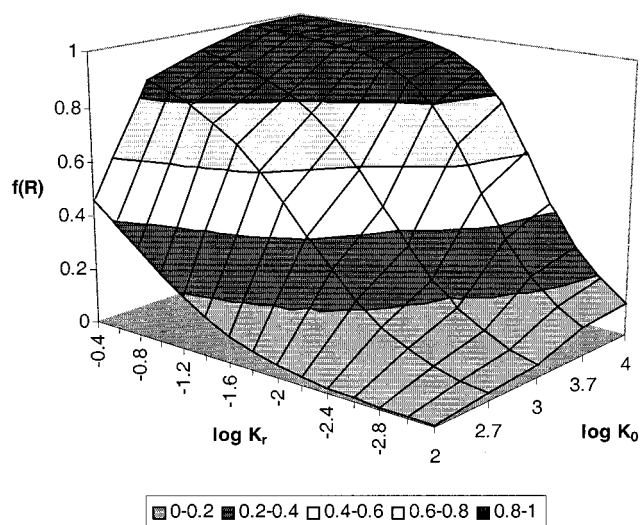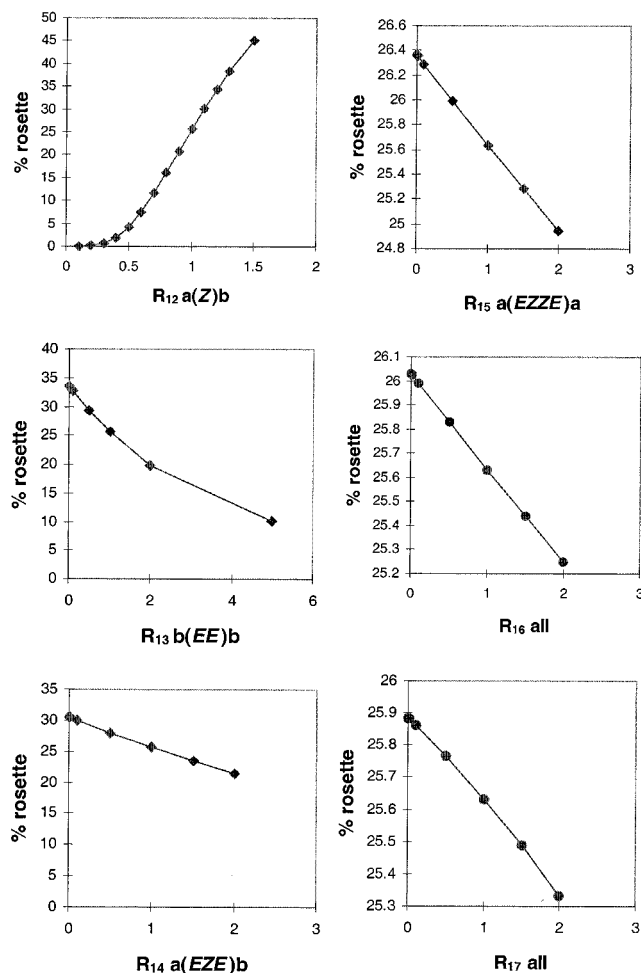
Figure 10. Effect of individual steric parameters ($R_{12}-R_{28}$) on percentage of rosette in an equilibrating mixture of free A, free B, tapes, and rosette.

importance of these interactions follows directly from statistics. In fact, the change in rosette fraction shows an almost linear relation with the number of occurrences for every steric parameter (see Table 1 and Figure 11).

The explanation of these results is not difficult after all. The effect of steric repulsions that exclusively occur in molecules other than the rosette ($R_{13}-R_{28}$) can affect the fraction of rosette only in an *indirect* manner, i.e., through changes in the concentrations of both free **1** and **2** (law of mass action). The reason these indirect effects are much smaller is that there are 271 different species in chemical equilibrium, representing the best buffer in the world! The capacity of this buffer is large enough to dilute the effect of sterics. For example, 101 structures of the 271 species do not suffer from any of the R_{13}-a(*EE*)a steric interactions mentioned (see Table 1). Even when all the steric repulsions that are only present in tapelike structures (i.e., $R_{13}-R_{28}$) are taken as 0.0001 (strong repulsion), the rosette fraction in the mixture changes only from 25% to 41%. In comparison to the much larger effects observed for changes in K_0 and K_r, it does not seem likely that variations in the steric repulsions in tapelike assemblies can be held responsible for the structural changes as observed by Whitesides and co-workers (for detailed discussion see below).[26,29,44]

Figure 9. 2D representation of the influence of both K_0 and K_r (logarithmic scales) on the fraction of rosette in an equilibrating mixture of free A, free B, tapes, and rosette.

repulsion) changes the rosette fraction from 25% to 33%. So, it seems possible to direct rosette formation by maximizing the steric repulsion in linear tapes, *but the effect is not very large*. The effect of the remaining steric interactions ($R_{14}-R_{28}$) is directionally the same as for R_{13}-a(*EE*)a, albeit that the magnitude of the steric effect is much smaller. The relative

Experimental Determination of K_0 and K_r

To link our model calculations to experimental values, it is necessary to have access to values for K_0 and K_r and to have
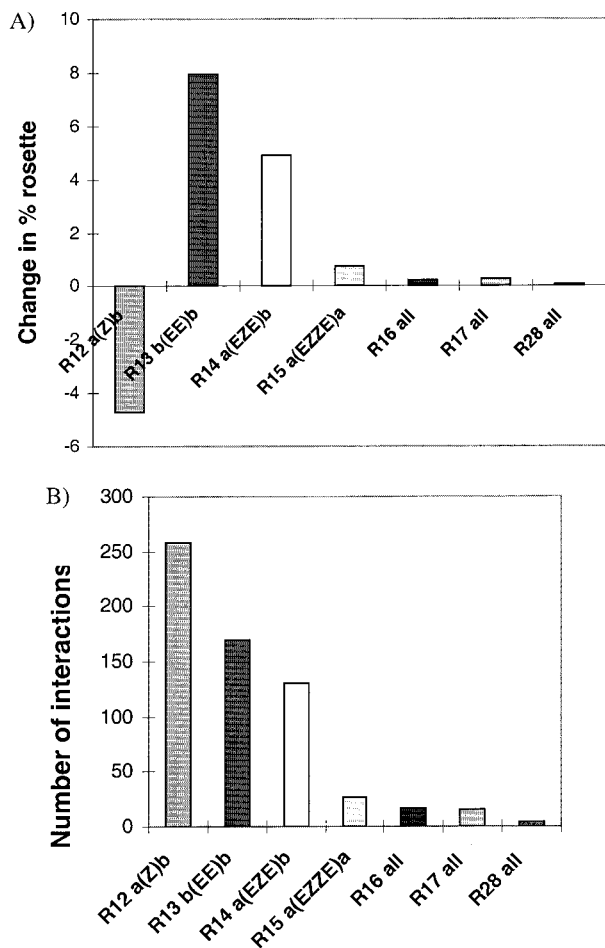
Figure 11. (A) Cumulative effect of steric parameters on percent rosette formation ($R_{12} = 0.9$, $R_{13}-R_{28} = 0.001$) in an equilibrating mixture of free A, free B, tapes, and rosette. (B) Number of molecules with at least one repulsive interaction.

Table 1. Occurrence Frequency of Different Types of Steric Interactions ($R_{12}-R_{28}$) and of Oligomeric Tapelike Hydrogen-Bonded Assemblies Composed of Differing Amounts of Melamine **1** and Cyanurate/Barbiturate **2**

steric parameter	no. of interactions per molecule	no. of molecules involved
R_{12}-a(Z)b	0	12
	1	28
	2	62
	3	70
	4	60
	5	28
	6	9 + R
	7	1
R_{13}-a(EE)a	0	101
	1	137
	2	29
	3	3
R_{14}-a(EZE)b	0	139
	1	108
	2	22
	3	1
R_{15}-a($EZZE$)a	0	244
	1	26
R_{16}-b($EZZZE$)a	0	253
	1	17
R_{17} all	0	254
	1	16
R_{28} all	0	266
	1	4

Table 2. ^{1}H NMR Chemical Shift Data for Various Melamine Derivatives That Were Used To Determine Experimental K_0 Values

compound	$\delta(H^1)^a$ (ppm)	$\delta(H^2)^a$ (ppm)
3a	7.366	
3b	6.575	4.670
3d	4.643	4.520
3f	6.594	
3g	4.598	
3h	6.688	5.124

^{a} Chemical shifts in CDCl$_3$ at 24 °C.

information on the effect of the different types of steric repulsions. We have experimentally determined a set of K_0 values, and our synthetic efforts have been geared toward the synthesis of melamine and cyanuric acid or barbituric acid derivatives **3** and **4** that can be used to determine values for K_r. The results of these experiments will be discussed first.

For an accurate determination of the interaction parameters between substituted melamine derivatives **3** and cyanurates or barbiturates **4**, it is necessary to quantify first the self-association of these compounds. To this end, samples dissolved in CDCl$_3$ were diluted, and from the change in NMR chemical shift of the NH and/or NH$_2$ signals (Table 2) the association constants for the homodimers were determined at 297 K. In general, the melamine derivatives **3** show little tendency to form hydrogen-bonded dimers, since the K_{dim} values obtained were in the range 0.1−1.0 M^{-1}. The cyanurate **4a** and the barbiturate **4b** form slightly more stable associates ($K_{dim} = 7.4 \pm 0.09$ and 1.7 ± 0.5 M^{-1}, respectively, at 297 K). Inclusion of self-association in the fitting procedures for their complexes has only a marginal effect (at most 3% change) on the K_0 values and was therefore neglected.

The basic association constant K_0 as required in our model description has been determined for cyanurate **4a** and barbiturate **4b** complexes with the melamine derivatives shown in Table 3. NMR titration and dilution experiments were conducted at 297 and 308 K. The values compare well with those reported by Würthner and co-workers.[9]

The interpretation of the observed changes in the NH chemical shift of the melamines and barbiturates requires some caution, because melamine derivatives consist of rotamers, and not all of them have the proper geometry to form H-bonded complexes.[9,45] When both rotamer interconversion and chemical exchange between free and complexed species is fast (case I), the normal (i.e., neglecting the presence of rotamers) fitting procedures can be used, and the obtained K_0 values refer to the mixture of rotamers. When rotamer interconversion is slow and chemical exchange is still fast (case II), this situation is the same as long as the barbiturate or cyanurate NH proton signals are used as a probe. However, when the melamine NH proton signal is used as a probe, a model must be used that includes all rotamers. The binding constants collected in Table 3 were obtained according to this approach and refer to the mixture of rotamers in all cases. To avoid the complications brought about by slowly interconverting rotamers in the interpretation of NMR spectra, binding constants were also determined by vapor pressure osmometry (VPO),[46] the values of which are not affected by the rates of the chemical processes. From the results in Table 3, it is clear that both techniques give very similar values. The maximum difference in K_0 values observed was a factor of 3.

(45) Willner, I.; Rosengaus, J.; Biali, S. *Tetrahedron Lett.* **1992**, *33*, 3805−3808.

(46) Higler, I.; Grave, L.; Breuning, E.; Verboom, W.; De Jong, F.; Fyles, T. M.; Reinhoudt, D. N. *Eur. J. Org. Chem.* **2000**, 1727−1734.

Table 3. Association Constants (K_0, M^{-1}) and Free Energies ($\Delta G°$, $kJ \cdot mol^{-1}$) Obtained by ^1H NMR Spectroscopy Titration ($CDCl_3$) and VPO ($ClCH_2CH_2Cl$, 35 °C) Dilution Experiments

	4a			4b		
	^1H NMR		VPO	^1H NMR		VPO
	24 °C	35 °C	35 °C	24 °C	35 °C	35 °C
3a	$CIS^a = 6.15$ (NH_{barb}) $K_0 = (1.1 \pm 0.1) \times 10^2$ $-\Delta G° = 11.6 \pm 0.3$	$CIS = 5.68$ (NH_{barb}) $K_0 = (0.8 \pm 0.2) \times 10^2$ $-\Delta G° = 11.2 \pm 0.5$	$K_0 = (1.2 \pm 0.15) \times 10^2$ $-\Delta G° = 12.2 \pm 0.3$	$CIS = 2.50$ (H^1) $K_0 = (5.1 \pm 0.6) \times 10^2$ $-\Delta G° = 15.4 \pm 0.3$	$CIS = 6.05$ (NH_{cyan}) $K_0 = (1.7 \pm 0.4) \times 10^2$ $-\Delta G° = 13.1 \pm 0.6$	$K_0 = (5.5 \pm 0.5) \times 10$ $-\Delta G° = 10.3 \pm 0.2$
3b	$CIS = 2.41$ (H^1) $CIS = 1.20$ (H^2) $K_0 = (5.3 \pm 0.4) \times 10^2$ $-\Delta G° = 15.5 \pm 0.2$	$CIS = 5.79$ (NH_{barb}) $CIS = 2.55$ (H^1) $CIS = 1.03$ (H^2) $K_0 = (2.6 \pm 0.4) \times 10^2$ $-\Delta G° = 14.2 \pm 0.3$	$K_0 = (1.1 \pm 0.15) \times 10^2$ $-\Delta G° = 12.1 \pm 0.3$	$CIS = 3.45$ (H^1) $K_0 = (4.2 \pm 1.0) \times 10^3$ $-\Delta G° = 20.6 \pm 0.5$	$CIS = 3.53$ (H^1) $CIS = 1.86$ (H^2) $K_0 = (1.2 \pm 0.1) \times 10^3$ $-\Delta G° = 18.1 \pm 0.3$	$K_0 = (5.7 \pm 0.8) \times 10^2$ $-\Delta G° = 16.2 \pm 0.4$
3d	$CIS = 2.60$ (H^1) $K_0 = (1.4 \pm 0.4) \times 10^2$ $-\Delta G° = 12.2 \pm 0.6$	$CIS = 6.37$ (NH_{barb}) $CIS = 3.20$ (H^1) $CIS = 1.42$ (H^2) $K_0 = (1.7 \pm 0.1) \times 10^2$ $-\Delta G° = 13.2 \pm 0.2$	$K_0 = (1.1 \pm 0.1) \times 10^2$ $-\Delta G° = 12.1 \pm 0.2$	$CIS = 4.46$ (H^1) $K_0 = (5.8 \pm 3.8) \times 10^3$ $-\Delta G° = 21.4 \pm 1.8$	$CIS = 4.25$ (H^1) $CIS = 2.13$ (H^2) $K_0 = (9.0 \pm 1.8) \times 10^3$ $-\Delta G° = 23.3 \pm 0.4$	$K_0 = (2.4 \pm 0.3) \times 10^3$ $-\Delta G° = 19.9 \pm 0.3$
3f	$CIS = 2.40$ (H^1) $K_0 = (2.8 \pm 0.2) \times 10^2$ $-\Delta G° = 13.9 \pm 0.2$	$CIS = 2.74$ (H^1) $K_0 = (4.9 \pm 0.5) \times 10$ $-\Delta G° = 10.0 \pm 0.2$	$K_0 = (1.3 \pm 0.2) \times 10^2$ $-\Delta G° = 12.5 \pm 0.4$	$CIS = 3.11$ (H^1) $K_0 = (3.4 \pm 0.9) \times 10^2$ $-\Delta G° = 14.4 \pm 0.8$	$CIS = 2.82$ (H^1) $K_0 = (2.5 \pm 0.5) \times 10^2$ $-\Delta G° = 14.1 \pm 0.5$	$K_0 = (2.3 \pm 0.3) \times 10^2$ $-\Delta G° = 13.9 \pm 0.3$
3g	$-\Delta G° = 13.9 \pm 0.3$	$CIS = 6.4$ (NH_{barb}) $CIS = 3.20$ ($NHCH_2$) $K_0 = (1.0 \pm 0.1) \times 10^2$ $-\Delta G° = 11.8 \pm 0.2$	$K_0 = (1.3 \pm 0.2) \times 10^2$ $-\Delta G° = 12.4 \pm 0.4$	$CIS = 4.51$ ($NHCH_2$) $K_0 = (3.9 \pm 0.9) \times 10^2$ $-\Delta G° = 14.7 \pm 1.6$	$CIS = 4.53$ ($NHCH_2$) $K_0 = (1.5 \pm 0.1) \times 10^4$ $-\Delta G° = 24.6 \pm 0.2$	$K_0 = (9.2 \pm 2.7) \times 10^3$ $-\Delta G° = 23.4 \pm 0.5$
3h	$CIS = 2.25$ (H^1) $CIS = 2.40$ (H^2) $K_0 = (2.2 \pm 0.2) \times 10^2$ $-\Delta G° = 13.3 \pm 0.2$	$CIS = 6.28$ (NH_{barb}) $CIS = 2.87$ (H^1) $CIS = 3.25$ (H^2) $K_0 = (1.1 \pm 0.2) \times 10^2$ $-\Delta G° = 12.0 \pm 0.5$	$K_0 = (5.2 \pm 0.4) \times 10$ $-\Delta G° = 10.1 \pm 0.1$	$CIS = 3.49$ (H^1) $CIS = 3.78$ (H^2) $K_0 = (5.3 \pm 0.5) \times 10^2$ $-\Delta G° = 15.5 \pm 0.3$	$CIS = 3.84$ (H^1) $CIS = 3.82$ (H^2) $K_0 = (7.3 \pm 1.2) \times 10^2$ $-\Delta G° = 16.9 \pm 0.4$	$K_0 = (7.6 \pm 1.1) \times 10^2$ $-\Delta G° = 17.0 \pm 0.3$

^{a} CIS = complexation induced shift.

Table 4. Association Constants (K, M^{-1}) and Complexation Induced Shifts (CIS, in ppm) Obtained by NMR ($CDCl_3$) at 24 °C for the Melamine−Cyanurate Complex $1d \cdot 4a_2$ and the Melamine−Barbiturate Complex $1d \cdot 4b_2$

$1d \cdot 4a_2$	$1d \cdot 4b_2$
$K_1 = 8400$ (fixed)	$K_1 = 1060$ (fixed)
$K_2 = 1850 \pm 700$	$K_2 = 160 \pm 50$
CIS(NH) = 1.21 (1:1)	CIS(NH) = 1.52 (1:1)
CIS(NH) = 2.32 (1:2)	CIS(NH) = 2.57 (1:2)
$CIS(NH_2) = 0.92$ (1:1)	$CIS(NH_2) = 1.13$ (1:1)
$CIS(NH_2) = 2.53$ (1:2)	$CIS(NH_2) = 2.68$ (1:2)

Table 5. Association Constants (K, M^{-1}) and Complexation Induced Shifts (CIS, in ppm) Obtained by NMR ($CDCl_3$) and VPO (Dichloroethane) for the Melamine−Barbiturate Complex $5b \cdot 2a$

^1H NMR (24 °C)	VPO (35 °C)
$CIS = 6.37$ (NH_{barb})	
$CIS = 2.11$ ($ArNH$)	
$CIS = 1.48$ ($BzNH$)	
$K = (3.6 \pm 1.4) \times 10^4$	$K = (1.1 \pm 0.15) \times 10^4$
$-\Delta G° = 25.9 \pm 0.8$	$-\Delta G° = 23.8 \pm 0.3$

From the results it is clear that the barbiturate forms rather weak (K_0 in the range $100-500M^{-1}$ at 24 °C) complexes with melamines (Table 3). In line with the higher acidity of the cyanurates,[15,47] their melamine complexes are more stable than barbiturates: K_0 values range from 300 to 5000 M^{-1}. This difference in complex stability between barbiturates and cyanurates seems to be larger for melamines having alkyl (**3d**, **3g**) instead of aryl (**3a**, **3b**) substituents.

The K_0 values determined above refer to complex formation between isolated H-bond donor and acceptor sites. In the model it is assumed that all K_0 values in the self-assembly process are the same (eqs 1−4). To test this assumption, the consecutive binding of barbiturate **4a** and cyanurate **4b** to the bifunctional melamine **1d** was studied. The number of unknown parameters, K_1, K_2, and the two NH chemical shifts in the 1:1 (δ_1) and the 1:2 (δ_2) complex, are too large to allow an accurate determination based on NMR titration experiments. Therefore, we assumed that the first binding constant of **1d** is the same as that of melamine **3a** (hence, $K_1(1d) = 2K_0(3a)$, the factor 2 being a statistical factor). This leads to the K_2, δ_1, and δ_2 values as shown in Table 4.

The values found for K_2 (160 and 1850 M^{-1} for barbiturate **4a** and cyanurate **4b**, respectively) are close to expectations

(47) Shieh, H.; Voet, D. *Acta Crystallogr., Sect. B: Struct. Sci.* **1976**, *32*, 2354−2360.

(530/2 and 4200/2 M^{-1}) based on statistics ($K_2 = K_0/2$). We therefore conclude that the assumption that each step in the self-assembly process can be described by the same basic binding constant K_0 is a valid one.

The direct determination of the macrocyclization constant K_r, from the equilibrium shown in eq 5 of the model, is rather difficult. The indirect route via eqs 6−9 is not easy either, since it would require the synthesis of a covalent rosette precursor. Therefore, we turned to eq 10, and estimated the binding constant K_{plug} for rosette formation from the monomer and the 5-mer ($i = 1$), for which we chose dimelamine **5b** as a model compound. The *m*-xylylene spacer unit in **5b** was carefully chosen on the basis of examination of molecular models, which show that this spacer approximates the positioning of the two melamine units in the single rosette assembly as closely as possible.

There is good evidence for formation of the **5b·2a** complex in the solid state. A white powder can be precipitated from an equimolar solution of **5b** and **2a** in aqueous ethanol and dichloromethane. Elemental analysis of the solid nicely corresponds to the 1:1 stoichiometry of the **5b·2a** complex.

The determination of the binding constant of the **5b·2a** complex was performed by titrating **5b** into a $CDCl_3$ solution of **2a** and monitoring the chemical shift changes of the NH proton signal of **2a** (Table 5). Fitting of the binding isotherm to a 1:1 complexation model gave a binding constant of (3.6 ±

1.2) $\times$ 10^4 M^{-1} ($\Delta G° = -25.9$ kJ·mol^{-1}).[48,49] From the K_{plug} value obtained for **5b** (3.6 $\times$ 10^4 M^{-1}) and the K_0 value obtained for the parent melamine **3h** (220 M^{-1}), it follows from eq 11 that the macrocyclization constant $K_r = 0.18 \pm 0.05$. Any attempts to determine the parameter K_r for cyanurates have failed, because association is too strong to obtain an accurate value. Molecular models suggest that the effective molarity for the ring-closing step will not be drastically different for cyanurates in comparison to that for barbiturates.

In conclusion, we can state that, at 24 °C, K_0 values for 1:1 complexes between crippled melamines **3** and crippled barbiturates/cyanurates **4** are in the range 100−500 M^{-1} for barbiturates (**4a**) and 300−5000 M^{-1} for cyanurates (**4b**), respectively. The effective molarity for the ring-closing step is assumed to be 0.18 in both cases.

Re-evaluation of the Covalent Preorganization and Peripheral Crowding Concepts

From the phenomenal work of the Whitesides group on hydrogen-bonded assemblies, two general concepts have emerged for the selective noncovalent synthesis of single rosettes. The first concept, viz. *covalent preorganization*,[18,50] involves the use of a Hub spacer (C_3 symmetry) to covalently connect the individual melamine units in a cyclic fashion, which strongly preorganizes these monomeric units for single rosette formation. In this way the number of different orientations of the melamine units is drastically reduced, and the formation of the cyclic single rosette is favored on entropic grounds.

When we consider these results in light of our model calculations, the concept of covalent preorganization is equivalent to maximizing the value of K_r. As the model calculations show (Figures 8 and 9), a value of $K_r \approx 1$ indeed leads exclusively to rosette formation. Several experimental studies have shown that the rigidity of the Hub spacer plays an important role.[51] Spacers that are too flexible do not sufficiently preorganize the components and lead to the formation of insoluble hydrogen-bonded polymers. A reduction in the rigidity of the covalent spacer can be viewed as equivalent to a reduction in the value of K_r, which does lead to a gradual decrease in the rosette fraction.

In another series of papers, the Whitesides group has put forward the concept of *peripheral crowding*,[26,29,44] which states that preferential formation of cyclic single rosettes in solution is primarily driven by repulsive steric interactions between the melamine units in the corresponding linear or crinkled tapes (R$_{1,3}$-a(*EE*)a, see Figure 5). Evidence for this comes from X-ray diffraction studies, which show that cyanuric acid−melamine assemblies without bulky substituents preferentially crystallize as tapes (from EtOH, CH$_3$CN, or THF),[28] while the cyanuric acid−melamine assembly containing the bulky *N,N′*-bis(*p-tert*-butylphenyl)-2,4,6-triamino-1,3,5-triazine crystallizes selectively as the cyclic rosette (toluene/isopropyl alcohol, 1:1 v/v).[29] Crystalline powders obtained from a variety of other solvents (CHCl$_3$, acetone, CH$_3$CN, or MeOH/THF) gave very similar X-ray diffraction patterns, indicating that also in these solvents the rosette structure was formed. In addition to this, solution-

phase studies in chloroform seemed to support this hypothesis. Furthermore, it was found that assemblies from *N,N′*-bis(4-*tert*-butylphenyl)-2,4,6-triamino-1,3,5-triazine are highly soluble in CHCl$_3$ (>100 mM), regarded as being evidence for rosette formation. For the nonbulky melamines (phenyl, methylphenyl, isopropylphenyl), precipitation is usually observed (solubility <2 mM in CHCl$_3$), which was taken as proof for the predominant presence of tapelike structures. However, our model calculations have clearly shown that steric factors that occur exclusively in the tapelike assemblies do not improve the rosette fraction to a great extent (maximum increase ∼16%, vide supra), which means that the concept of steric crowding needs a serious re-evaluation.
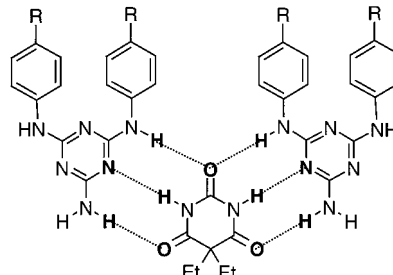
In principle, the concept of peripheral crowding as defined by Whitesides is based on two different assumptions. First, it is assumed that solid-state data can be used to estimate the thermodynamic stability of two (or more) equilibrating species in solution. Second, it is believed that the cyclic rosette has a much higher solubility than the corresponding tapelike structures, which have sticky polar ends that enormously reduce the solubility in apolar solvents. These two assumptions are, however, in contradiction, since the first assumption can be valid only when the solubilities of both tapes and rosettes are more or less comparable. In case they are very different (assumption 2), then the least soluble assembly, in this case the tape, would crystallize first, even if it is present in solution to a minor extent. An illustrative example of this was provided by Högberg, who reported the almost quantitative conversion of the *cis−trans−trans* to the *all-cis* isomer of calix[4]arene resorcinarenes by selective crystallization of the latter, which is initially only present in solution to a minor extent.[52,53] In light of these facts, it seems that the formation of tapelike structures in the solid state is more likely to be due to their much lower solubility, rather than a result of their higher thermodynamic stability. Following Högberg's case, the quantitative formation of tapes in the solid state can occur, even if the rosette is the predominant species in solution. However, the question remains why in case of the *N,N′*-bis(*p-tert*-butylphenyl)-2,4,6-triamino-1,3,5-triazine-containing assemblies the rosette structure precipitates first, when we know that the maximum increase in rosette fraction due to R$_{13}$-a(*EE*)a is only ∼8%. The only possibility left is that substitution of the methyl substituents in **1a** for *tert*-butyl substituents, as in **1d**, strongly affects the relative solubility of the tape and rosette structures, either by increasing the solubility of the tapes or by decreasing the solubility of the rosette structure. To study this hypothesis in more detail, we carried out a series of computer simulation studies, in which we studied the effect of changing the melamine substituents on the shape and thermodynamic stability of the corresponding rosette and tapelike assemblies.

Gas-Phase Molecular Simulations

A series of gas-phase molecular simulations on four different 2:1 complexes **1$_2$·2a**, for which the steric bulk of the para-substituent of melamine **1** is gradually increased from methyl (**1a**), to ethyl (**1b**), to isopropyl (**1c**), to *tert*-butyl (**1d**), was performed. First, we studied whether the increase in steric bulkyness of the substituent has an effect on either the hydrogen bond distances or the angles of these hydrogen bonds with the plane of the tape. If steric hindrance between the melamine substituents in tapes (R$_{13}$-a(*EE*)b) would seriously affect the

(48) For this value of K_{plug} ($K_0 = 390$ M^{-1}, $K_c = 23$ M^{-1}), it can be shown that the linear species (in addition to the cycle R, the oligomers AB and AB$_2$ can be formed also) play no role in the titration experiment.

(49) By comparison, binding of **2a** to the Hamilton acyclic cleft gave a K_a value of 2.08 $\times$ 10^4 M^{-1} in CDCl$_3$,[62] very similar in magnitude to our value.

(50) Seto, C. T.; Whitesides, G. M. *J. Am. Chem. Soc.* **1993**, *115*, 1330−1340.

(51) Seto, C. T.; Mathias, J. P.; Whitesides, G. M. *J. Am. Chem. Soc.* **1993**, *115*, 1321−1329.
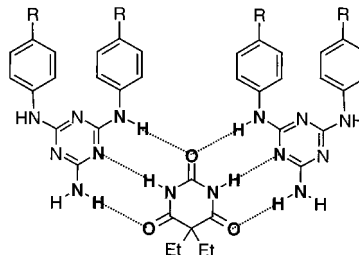
(52) Högberg, A. G. S. *J. Am. Chem. Soc.* **1980**, *102*, 6046−6050.

(53) Timmerman, P.; Verboom, W.; Reinhoudt, D. N. *Tetrahedron* **1996**, *52*, 2663−2704.

Table 6. Hydrogen Bond Distances in the 2:1 Hydrogen-Bonded Complexes $1_2 \cdot 2a$ As Determined from Gas-Phase-Minimized Structures (CHARMm 24.0)[a]

	HN*H*- - -O=C (Å)	N- - -HN(C=O)$_2$ (Å)	R$_2$N*H*- - -O=C (Å)
$1a_2 \cdot 2a$	1.989 (5)	2.079 (10)	1.939 (4)
$1b_2 \cdot 2a$	2.032 (13)	2.041 (15)	1.928 (6)
$1c_2 \cdot 2a$	2.003 (1)	2.051 (1)	1.944 (0)
$1d_2 \cdot 2a$	1.997 (3)	2.098 (42)	1.937 (3)

[a] The values given are averages of two measured values; numbers in parentheses indicate variations.

Table 7. Hydrogen Bond Angles (in the Plane *Perpendicular* to the Plane of the Tape) in 2:1 Hydrogen-Bonded Complexes $1_2 \cdot 2a$ As Determined from Gas-Phase-Minimized Structures (CHARMm 24.0)[a]

	H*N*—*H*- - -O=C (deg)	N- - -H—N(C=O)$_2$ (deg)	R$_2$*N*—*H*- - -O=C (deg)
$1a_2 \cdot 2a$	168.9 (5)	147.4 (14)	172.4 (27)
$1b_2 \cdot 2a$	173.4 (5)	157.3 (53)	172.4 (21)
$1c_2 \cdot 2a$	178.2 (1)	153.8 (4)	177.9 (1)
$1d_2 \cdot 2a$	168.8 (60)	143.2 (88)	167.7 (82)
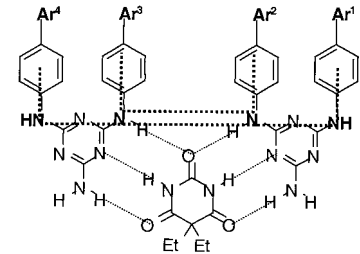
[a] The values given are averages of two measured values; numbers in parentheses indicate variations.

thermodynamic stability of these species, one would expect a significant change in either the hydrogen bond distances or angles. Our calculations show the following results.

For the four different complexes, the variation in N*H*- - -N and N*H*- - -O hydrogen bond distances is <0.05 Å (see Table 6). Moreover, the longest H-bond distances are not necessarily found for $1d_2 \cdot 2a$, which indicates that there seems to be no relationship between steric bulk of the substituent and the hydrogen bond distances. Furthermore, the angles of hydrogen bonds (in the plane *perpendicular* to the plane of the tape) in the complexes differ in general only by <10° (one exception of 14°, see Table 7). Although the shortest angles generally apply to the sterically bulkiest complex $1d_2 \cdot 2a$, it is very unlikely that the thermodynamic energies for these complexes differ much on the basis of the H-bond angle difference, because H-bond energies generally do not show a very strong angle dependency.[54]

In addition to this, we studied how an increase in the volume of the melamine substuent affects the shape of the 2:1 assemblies

(54) Schuster, P.; Zundel, G.; Sandorfy, C. *The Hydrogen Bond: Recent Developments in Theory and Experiments*; North-Holland: Amsterdam, The Netherlands, 1976; Vols. 1−3.

Table 8. Dihedral Angles in 2:1 Hydrogen-Bonded Complexes $1_2 \cdot 2a$ As Determined from Gas-Phase-Minimized Structures (CHARMm 24.0)

	Ar^2—N- - -N—Ar^3 (deg)	Ar^1—N- - -N—Ar^4 (deg)	Ar^1—N- - -N—Ar^2 (deg)
$1a_2 \cdot 2a$	13.1	18.3	13.9
$1b_2 \cdot 2a$	7.9	10.2	10.8
$1c_2 \cdot 2a$	5.9	29.2	12.3
$1d_2 \cdot 2a$	29.2	79.4	24.1

$1_2 \cdot 2a$ and the cyclic rosette $1_3 \cdot 2a_3$. The calculations (see Table 8 and Figure 12) clearly show that an increase in the volume of the melamine substituents strongly affects the shape of the $1_2 \cdot 2a$ complexes. For example, when comparing the average dihedral angles for the Ar$_2$—N- - -N—Ar$_3$, the Ar$_1$—N- - -N—Ar$_4$, and the Ar$_1$—N- - -N—Ar$_2$ bonds for the three 2:1 complexes $1_2 \cdot 2a$, $1_2 \cdot 2b$, and $1_2 \cdot 2c$ (9°, 19°, and 12°) with that of $1_2 \cdot 2d$ (29°, 79°, and 24°), it becomes immediately clear that the latter structure is severely distorted from planarity. Visualization of these calculations is depicted in Figure 12. For the corresponding cyclic rosettes $1_3 \cdot 2a_3$, the bulky substituents are too far apart to be able to cause a deviation from planarity.

These calculations thus show that the strength of the H-bonds in terms of bond distance and bond angles, and therefore the thermodynamic stability, seems not to be affected much. However, the flatness of the tapelike structures is lost as a result of steric hindrance between bulky substituents on the melamines. In the solid state, the flatness of the structure plays an important role in terms of crystal packing efficiency. Nonflat structures (in this case the linear tapes) do not pack as efficiently as flat structures (in this case the cyclic rosette). This observation can provide a suitable explanation for the observed preferential crystallization of rosette $1d_3 \cdot 2a_3$, because in that case the solubility of the corresponding tapelike structures has been largely increased as a result of steric strain.

Experimental Verification of Model Calculations

To verify the predictions of our model by experimental evidence, we have thoroughly investigated the assembly behavior of a variety of melamines **1** with barbituric acid or cyanuric acid derivatives **2** in apolar solvents, like chloroform and toluene. As mentioned before, such measurements are strongly hampered by the fact that the solubility of certain assemblies (most likely tapelike structures) is too low in these solvents to allow us to study the assemblies under homogeneous conditions. For those assemblies that remained homogeneous under these conditions, we observed rapid exchange of the individual components on the ^{1}H NMR chemical shift time scale. This made it impossible to determine individually the amount of tapes and rosette in an equilibrating mixture of **1** and **2**. Attempts to study these assemblies under typically slow exchange conditions (chloroform, −50 °C; toluene, 0 °C) all failed, because of strong nonspecific aggregation ("stacking") of the assemblies at these temperatures.

Therefore, we focused our attention to the "rosette" system $1d_3 \cdot 2a_3$ that has been studied in solution by Whitesides using
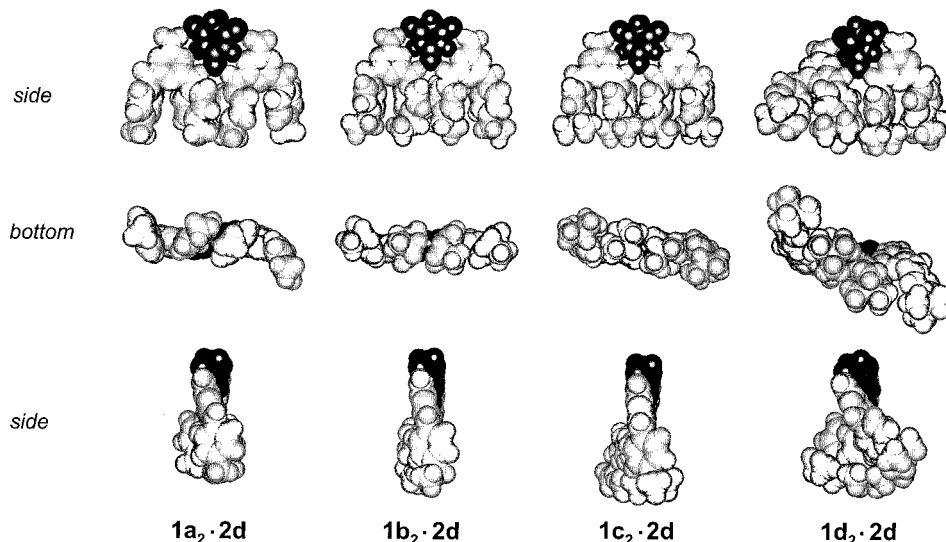
Figure 12. Different views of the 2:1 melamine−barbiturate assemblies **1$_2$·2a** showing the effect of the volume of the melamine substituents on the shape of the assembly (for quantitative interpretation of these results, see Tables 6−8).
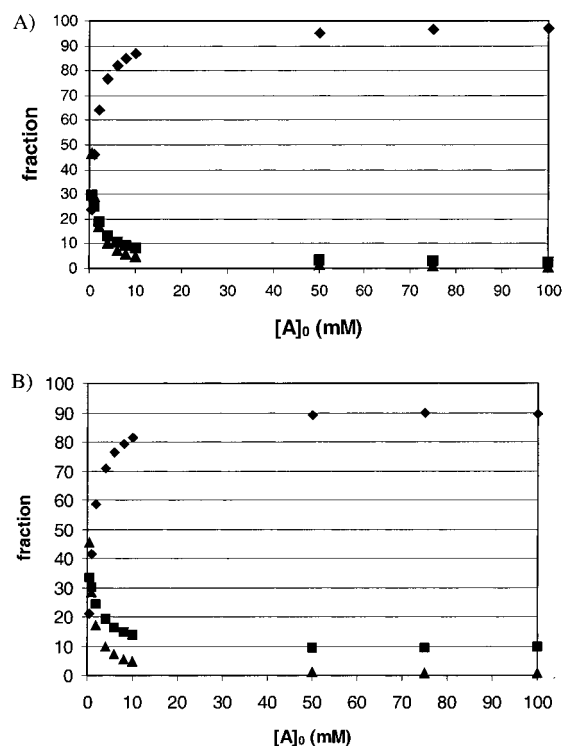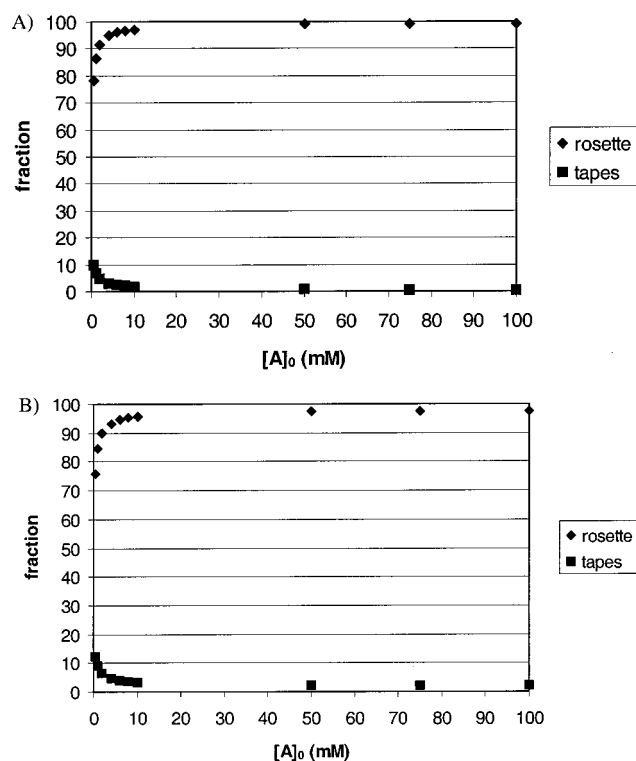

Figure 13. Composition of an equilibrating mixture of **1d** and **2a** in CDCl$_3$ (K_0 = 530 M^{-1}, K_r = 0.18) with varying concentration [A]$_0$ = [B]$_0$ as calculated using our model. Conditions: (A) R$_{13}$−R$_{28}$ = 0.0001 (strong repulsion), R$_{12}$-a(Z)b = 1 (no repulsion); (B) R$_{12}$−R$_{28}$ = 1 (no repulsion).

Figure 14. Composition of an equilibrating mixture of **1d** and **2b** in CDCl$_3$ (K_0 = 2500 M^{-1}, K_r = 0.18) with varying concentration [A]$_0$ = [B]$_0$ as calculated using our model. Conditions: (A) R$_{13}$−R$_{28}$ = 0.0001 (strong repulsion), R$_{12}$-a(Z)b = 1 (no repulsion); (B) R$_{12}$−R$_{28}$ = 1 (no repulsion).

both ^{1}H NMR spectroscopy and VPO measurements.[29] Simulation of the composition of this mixture using the experimentally determined K_0 and K_r values ((K_0 = 530 M^{-1}, K_r = 0.18, see Table 3) under "maximum repulsion" conditions (Figure 13A) clearly confirms Whitesides's conclusions that the assembly is mainly present as the cyclic rosette (98% maximum). The assembly stays intact at concentrations >10 mM but starts to dissociate significantly below this concentration. Simulation of the same system under "no repulsion" conditions (Figure 13B), representative for a mixture of **1a−c** and **2a** in CDCl$_3$, clearly shows that the composition of the mixture has hardly changed.

Typically, the fraction of tapes is ∼7−8% higher at most concentrations, at the expense of rosette (90% maximum).

In addition to this, we performed similar simulations for an equilibrating mixture of melamines **1** and cyanurate **2b** in CDCl$_3$ (K_0 = 2500 M^{-1}, K_r = 0.18). The results clearly show that the difference in rosette fraction under "no repulsion" and "maximum repulsion" conditions has been reduced to only 2−3% at maximum (Figure 14), which means that under these conditions the influence of steric interactions is almost gone. According to these model calculations, 1:1 mixtures of melamines **1** and cyanurates **2** are almost exclusively present as rosettes, with less than 3% of tapes being present. The experimentally

observed precipitation should therefore be due to the very low solubilities of the tapelike structures, which ultimately shift the thermodynamic equilibrium completely in favor of the least soluble products.

Conclusions

This paper describes model calculations for the assembly behavior of *N,N*-disubstituted melamines **1** and 5,5-disubstituted barbituric acid derivatives or *N*-substituted cyanuric acid derivatives **2** into linear and crinkled tapes [**1·2**]$_n$ and a cyclic rosette structure **1**$_3$·**2**$_3$. The model shows that the formation of rosettes vs tapes is primarily controlled by the two thermodynamic parameters, i.e., K_0, the basic association constant for a single melamine and cyanurate, and K_rK_0, the formation constant for the cyclic rosette from the isomeric linear hexamer. An increase in K_0 and K_r strongly increases the concentration of rosette over tapelike structures. Furthermore, it was found that steric repulsions within the tapelike structures (mainly R$_{13}$-a(*EE*)b) have only a minor effect on the fraction of rosette in the equilibrating mixture. Even if all possible steric interactions are maximized, the model predicts a maximum increase of only ~16% of the rosette fraction. In sharp contrast to this, the model predicts a strong sensitivity for the steric paramter R$_{12}$-a(*Z*)b, representing attractive and repulsive interactions between substituents of the melamine and cyanurate components. In light of these predictions, the concept of peripheral crowding as put forward by Whitesides has been re-evaluated. It seems likely that the solubility differences for tapelike structures with bulky and nonbulky substituents, as a result of the nonplanarity of the former, provide a suitable explanation for the preferential crystallization of the rosette in the case of bulky substituents on the melamine. Gas-phase simulations have indeed shown that the planarity of short tapes is lost upon increasing the size of the melamine substituents.

Experimental Section

General. Melting points were determined with a Gallenkamp melting point apparatus and are uncorrected. Microanalyses were performed by the chemical analysis unit of the University of Twente. ^{1}H NMR spectra were recorded on a Bruker AC 250 (250 MHz) or a Varian Unity 400 (400 MHz) spectrometer. Residual solvent protons were used as an internal standard. ^{1}H NMR data are reported as follows: chemical shifts (δ) measured in parts per million (ppm) downfield from tetramethylsilane (TMS); multiplicity; proton count. Multiplicities are reported as singlet (s), broad singlet (br s), doublet (d), triplet (t), and multiplet (m). ^{1}H and ^{13}C NMR spectra were recorded on a Bruker AC 250 (62.89 MHz) or a Varian 300 MHz spectrometer. ^{13}C chemical shifts (δ) are reported in ppm downfield from TMS, and identifiable signals are given. Assignment was determined with the aid of 90° and 135° DEPT experiments. FAB mass spectra were recorded on a Finnigan MAT90 spectrometer using *m*-nitrobenzyl alcohol (NBA) as a matrix. EI mass spectra were recorded on a Finnigan MAT90 spectrometer with an ionizing voltage of 70 eV. Chromatography was performed using gravity columns packed with Merck silica gel 60 (230−400 mesh). Anhydrous THF was distilled from Na/benzophenone immediately prior to use. Ethyl acetate was distilled from potassium carbonate. Dichloromethane, chloroform, and petroleum ether (60−80 °C) were distilled from calcium chloride. DMF was dried and stored over 4 Å molecular sieves. The synthesis of melamine derivative **1d**[29] and cyanurate derivative **2b**[50] was performed according to literature procedures.

Vapor Pressure Osmometry (VPO) Studies. VPO measurements were performed using Osmomat 070. Stock solutions were prepared gravimetrically (the complex components were weighted separately in 1:1 molar ratios), diluted volumetrically to a series of four solutions. All measurements for K_0 and K_{plug} were performed either in 1,2-

dichloroethane or in 1,2-dichloroethane/chloroform mixtures. Calculation of the K_0 values was performed according to the method described earlier.[46]

Binding Studies. The self-association behavior was measured by observing the NH chemical shift changes with concentration in CDCl$_3$ (dried over molecular sieves) at 24 °C. The resulting binding isotherm was fitted to a 1:1 self-association model to give a dimerization constant. Titrations were performed in CDCl$_3$ at 24 °C in duplicate and the results averaged to give the final constant. Each titration comprised 10 samples prepared by titrating a CDCl$_3$ solution containing the probe and titrant into a CDCl$_3$ solution of the probe alone, thus ensuring a constant concentration of probe in each sample. The chemical shifts of the NH proton indicated in Table 3 were used to fit a 1:1 binding model using a nonlinear least-squares fitting analysis. The solutions used were 5 mM or less in probe to minimize self-association, and the binding model did not incorporate dimerization into the calculated chemical shift.

Synthesis. 4-Amino-6-chloro-2-(4′-*tert*-butylanilino)-1,3,5-triazine (3a). A solution of 4-*tert*-butylaniline (1.86 g, 12.5 mmol) in THF (5 mL) was added dropwise over 5 min to an ice-cooled solution of cyanuric chloride (2.3 g, 12.5 mmol) and DIPEA (5 mL) in tetrahydrofuran (20 mL). The resulting yellow suspension was stirred for 2 h and then allowed to warm to room temperature, followed by bubbling of gaseous NH$_3$ through the solution for 2.5 h. Addition of H$_2$O (50 mL) gave a precipitate that was purified by column chromatography (SiO$_2$; CHCl$_3$/MeOH 9:1) to give **3a** as a white solid (4.89 g, 99%).
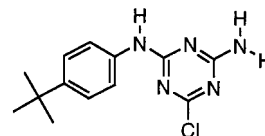
An analytically pure sample of **3a** was obtained by recrystallization from CH$_2$Cl$_2$/hexane. Mp 228−229 °C; MS (FAB) *m/z* 278.1 (M + H);^{1}H NMR (250 MHz, CDCl$_3$) δ 1.32 (s, 9H), 5.35 (br s, 2H), 7.08 (br s, 1H), 7.35−7.39 (m, 2H), 7.42−7.46 (m, 2H); ^{13}C NMR (62.5 MHz, DMSO-d_6) δ 31.2 (CH$_3$), 34.0 (C), 120.4 (CH), 125.1 (CH), 136.1 (C), 145.3 (C), 163.9 (C), 166.9 (C), 168.3 (C). Anal. Calcd for C$_{13}$H$_{16}$N$_5$Cl: C, 56.21; H, 5.81; N, 25.22. Found: C, 56.76; H, 5.76; N, 24.31.

4-Amino-6-dibutylamino-2-(4′-*tert*-butylanilino)-1,3,5-triazine (3b). A solution of **3a** (1:1 CHCl$_3$−solvate, 635 mg, 1.60 mmol), DIPEA (3 mL), and dibutylamine (1 mL) in THF (5 mL) was refluxed for 15 h. The reaction mixture was poured into CHCl$_3$ and washed with H$_2$O (2 × 50 mL), dried on MgSO$_4$, and evaporated under reduced pressure to
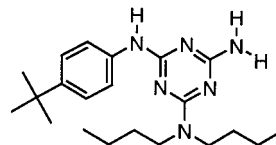
give a yellow oil. Purification by column chromatography (SiO$_2$; CHCl$_3$/MeOH 9:1) gave **3b** as a colorless gum (513 mg, 81%). MS (FAB) *m/z* 371.2 (M + H); ^{1}H NMR (250 MHz, CDCl$_3$) δ 0.93−0.98 (m, 6H), 1.30 (s, 9H), 1.30−1.40 (m, 4H), 1.50−1.62 (m, 4H), 3.46−3.52 (m, 4H), 4.68 (br s, 2H), 6.65 (br s, 1H), 7.26−7.30 (m, 2H), 7.49−7.52 (m, 2H); ^{13}C NMR (62.5 MHz, CDCl$_3$) δ 14.0 (CH$_3$), 20.2 (CH$_2$), 20.4 (CH$_2$), 30.1 (CH$_2$), 31.4 (CH$_2$), 34.2 (C), 46.6 (CH$_2$), 47.2 (CH$_2$), 119.6 (CH), 125.4 (CH), 137.0 (C), 145.1 (C), 164.4 (C), 165.4 (C), 166.9 (C). Anal. Calcd for C$_{21}$H$_{34}$N$_6$·0.25H$_2$O: C, 67.25; H, 9.27; N, 22.41. Found: C, 67.68; H, 9.12; N, 22.05.
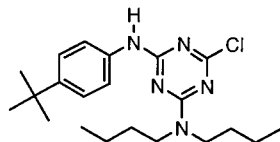
2-Amino-4-butylamino-6-dibutylamino-1,3,5-triazine (3d). A solution of *n*-butylamine (0.12 mL, 1.2 mmol) in THF (5 mL) was added dropwise over 5 min to an ice-cooled solution of cyanuric chloride (0.22 g, 1.2 mmol) and DIPEA (0.5 mL) in tetrahydrofuran (5 mL). The resulting suspension was stirred for 2 h and then allowed to warm to room temperature, followed by bubbling of gaseous NH$_3$ through the solution for 2.5 h. Addition of H$_2$O (50 mL) gave the chlorotriazine **3c** as a white precipitate that was filtered off and dried under vacuum. Next **3c** was dissolved in THF (5 mL), dibutylamine (500 mg, 3.87

mmol) and DIPEA (0.5 mL) were added, and the resulting solution was refluxed for 24 h. The solution was evaporated in vacuo and the residue dissolved in CHCl$_3$ (50 mL), washed with H$_2$O (3 × 50 mL), dried on MgSO$_4$, and evaporated in vacuo to give a colorless oil.
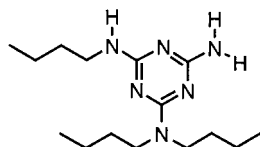

Purification by column chromatography (SiO$_2$; CHCl$_3$/MeOH 9:1) afforded **3d** as a colorless oil (282 mg, 80%). MS (FAB) *m/z* 295.2 (M + H); ^{1}H NMR (250 MHz, CDCl$_3$) δ 0.89−0.95 (m, 9H), 1.23−1.43 (m, 6H), 1.47−1.55 (m, 6H), 3.29−3.37 (m, 2H), 3.45 (t, *J* = 7.0 Hz, 4H), 4.58 (br s, 2H), 4.70 (br s, 1H); ^{13}C NMR (62.5 MHz, CDCl$_3$) δ 13.8 (CH$_3$), 14.0 (CH$_3$), 20.2 (CH$_2$), 30.1 (CH$_2$), 32.0 (CH$_2$), 40.3 (CH$_2$), 46.3 (CH$_2$), 165.2 (C), 166.1 (C), 166.9 (C). Anal. Calcd for C$_{15}$H$_{30}$N$_6$: C, 61.18; H, 10.27; N, 28.55. Found: C, 61.51; H, 10.51; N, 28.70.

4-Chloro-2-(4′-*tert*-butylanilino)-6-dibutylamino-1,3,5-triazine (3e). A solution 4-*tert*-butylaniline (0.86 g, 5.76 mmol) in THF (5 mL) was added dropwise to an ice-cooled solution of cyanuric chloride (1.06 g, 5.75 mmol) and DIPEA (2 mL) in THF (10 mL). The reaction was stirred for 5 h and allowed to warm to room temperature, and a solution of dibutylamine (0.78 g, 6.03 mmol) in THF (1 mL) was added dropwise. Stirring was continued at room temperature for 20 h, and the solvent was removed in vacuo. The residue was dissolved in CH$_2$-

Cl$_2$ (100 mL), washed with H$_2$O (2 × 50 mL) and HCl (1 M, 50 mL), dried on MgSO$_4$, and evaporated in vacuo to give an orange oil which was purified by column chromatography (hexane/ethyl acetate, 4:1) to give **3e** as a colorless oil (1.95 g, 87%). MS (FAB) *m/z* 390.3 (M + H); ^{1}H NMR (250 MHz, CDCl$_3$) δ 0.92−0.99 (m, 6H), 1.31 (s, 9H), 1.31−1.42 (m, 4H), 1.55−1.63 (m, 4H), 3.47−3.58 (m, 4H), 6.98 (br s, 1H), 7.30−7.34 (m, 2H), 7.46−7.50 (m, 2H).

2,4-Bis-(4′-*tert*-butylanilino)-6-dibutylamino-1,3,5-triazine (3f). A solution of 2,4-bis-(4′-*tert*-butylanilino)-6-chloromelamine (540 mg, 1.31 mmol)[55] and dibutylamine (1 mL) in THF (20 mL) was refluxed for 21 h. H$_2$O was then added, and the resulting amorphous solid was filtered. Recrystallization from CHCl$_3$/hexane gave **3f** as fine white
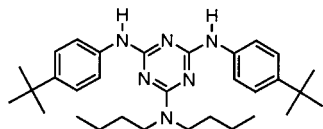
needles (438 mg, 67%). Mp 188−189 °C; MS (FAB) *m/z* 503.4 (M + H); ^{1}H NMR (250 MHz, CDCl$_3$) δ 0.99 (t, *J* = 7.3 Hz, 6H), 1.33 (s, 18H), 1.33−1.48 (m, 4H), 1.61−1.73 (m, 4H), 3.56 (t, *J* = 7.9 Hz, 4H), 7.16 (br s, 2H), 7.26−7.32 (m, 4H), 7.49−7.52 (m, 4H); ^{13}C NMR (62.5 MHz, CDCl$_3$) δ 14.1 (CH$_3$), 20.4 (CH$_2$), 30.1 (CH$_2$), 31.5 (CH$_3$), 34.2 (C), 47.4 (CH$_2$), 119.7 (CH), 125.4 (CH), 136.9 (C), 145.2 (C), 164.1 (C), 165.1 (C). Anal. Calcd for C$_{31}$H$_{46}$N$_6$: C, 74.06; H, 9.22; N, 16.72. Found: C, 73.97; H, 9.07; N, 16.84.

2,4-Bis(butylamino)-6-dibutylamino-1,3,5-triazine (3g). 1-Aminobutane (1 mL) was added dropwise to a solution of cyanuric chloride (0.21 g, 1.125 mmol) in THF (10 mL). The solution was stirred at room temperature for 24 h, and then HCl (1 M, 20 mL) was added. The resulting precipitate was filtered, washed with HCl (1 M, 10 mL) and H$_2$O (10 mL), and dried under vacuum. The solid was then

(55) Mathias, J. P.; Seto, C. T.; Simanek, E. E.; Whitesides, G. M. *J. Am. Chem. Soc.* **1994**, *116*, 1725−1736.

dissolved in dibutylamine (10 mL) and refluxed overnight, whereafter the excess of dibutylamine was evaporated under reduced pressure. The remaining yellowish residue was dissolved in chloroform, washed with H$_2$O (3 × 50 mL), dried on Na$_2$SO$_4$, and evaporated to dryness to give a yellow oil. Purification by preparative TLC (SiO$_2$, chloroform/
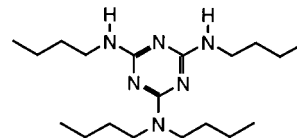

methanol 9:1) gave pure **3g** (0.33 g, 83%). MS (FAB) *m/z* 351.4 (100%, [M + H]$^+$); ^{1}H NMR δ 4.63 (br s, 2H, NH), 3.40 (t, 4H, *J* = 7.6 Hz, CH$_2$), 3.27 (q, 4H, *J* = 7.0 Hz, CH$_2$), 1.6−1.4 (m, 8H, CH$_2$), 1.4−1.2 (m, 8H, CH$_2$), 0.85 (2t,12H, *J* = 7.6 Hz, CH$_3$). Anal. Calcd for C$_{19}$N$_6$H$_{38}$: C, 65.10; N, 24.00; H, 10.90. Found: C, 65.24; N, 24.05; H, 10.83.

2-Benzylamino-4-(4′-*tert*-butylanilino)-2-dibutylamino-1,3,5-triazine (3h). A solution of **3e** (1.14 g, 2.92 mmol), DIPEA (2 mL), and benzylamine (1 mL) in THF was refluxed for 23 h. The solvent was evaporated under reduced pressure, and the residue was dissolved in CH$_2$Cl$_2$ (100 mL), washed with HCl (1 M, 25 mL), H$_2$O (50 mL), and brine (25 mL), and dried MgSO$_4$. Evaporation under reduced pressure
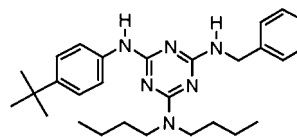

gave a colorless oil that was further purified by column chromatography (SiO$_2$; CHCl$_3$/MeOH 95:5) to give **3h** as a colorless gum (1.08 g, 80%). MS (FAB) *m/z* 461.3 (M + H); ^{1}H NMR (250 MHz, CDCl$_3$) δ 0.90−1.01 (m, 6H), 1.31 (s, 9H), 1.31−1.43 (m, 4H), 1.53−1.64 (m, 4H), 3.50 (m, 4H), 4.59 (d, *J* = 5.8 Hz, 2H), 5.41 (br s, 1H), 7.06 (br s, 1H), 7.25−7.33 (m, 7H), 7.49−7.53 (m, 2H); ^{13}C NMR (62.5 MHz, CDCl$_3$) δ 14.1 (CH$_3$), 20.3 (CH$_2$), 20.5 (CH$_3$), 30.2 (CH$_2$), 31.5 (CH$_2$), 34.2 (C), 44.6 (CH$_2$), 46.8 (CH$_2$), 47.2 (CH$_2$), 119.4 (CH), 125.4 (CH), 127.0 (CH), 127.5 (CH), 128.5 (CH), 137.2 (C), 139.8 (C), 144.8 (C), 164.2 (C), 165.1 (C), 166.0 (C). Anal. Calcd for C$_{28}$H$_{40}$N$_6$·0.5H$_2$O: C, 71.60; H, 8.80; N, 17.90. Found: C, 71.93; H, 8.72; N, 17.91.

2,4-Bis(heptylamino)-6-chloro-1,3,5-triazine (3i). 1-Aminoheptane (5 mL) was added dropwise to a solution of cyanuric chloride (2.21 g, 12 mmol) in THF (20 mL). The solution was stirred at room temperature for 24 h, and then HCl (1 M, 50 mL) was added. The resulting
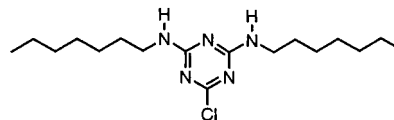
precipitate was filtered, washed with HCl (1 M, 10 mL) and H$_2$O (10 mL), and recrystallized from CHCl$_3$ to give **3i** as a white solid (2.1 g, 51%). Mp 164−165 °C; MS (FAB) *m/z* 342.4 (M + H); ^{1}H NMR (250 MHz, CDCl$_3$) δ 0.85−0.91 (m, 6H), 1.28−1.30 (m, 16H), 1.54−1.60 (m, 4H), 3.36−3.44 (m, 4H), 5.52 (br s, 2H).

2,4-Bis(*N*-heptylamino)-6-dibutylamino-1,3,5-triazine (3j). A solution of **3i** (302 mg, 0.88 mmol) and dibutylamine (2 mL) in THF (5 mL) was refluxed for 27 h. The solvent was evaporated under reduced pressure, and then the residue was dissolved in CHCl$_3$ (50 mL), washed with H$_2$O (50 mL) and HCl (1 M, 50 mL), and dried on MgSO$_4$. Evaporation of the solvent under reduced pressure gave a pale yellow gum, which was purified by column chromatography (SiO$_2$; hexane/
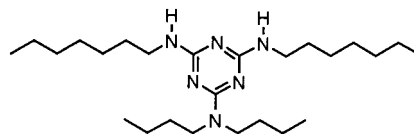
EtOAc, 4:1) to give pure **3j** as a colorless oil (181 mg, 47%). MS (FAB) *m/z* 435.3 (M + H); ^{1}H NMR (250 MHz, CDCl₃) δ 0.85−0.96 (m, 12H), 1.27−1.35 (m, 20H), 1.52−1.59 (m, 8H), 3.28−3.43 (m, 4H), 3.46 (t, *J* = 7.3 Hz, 4H), 4.57 (br s, 2H); ^{13}C NMR (62.5 MHz, CDCl₃) δ 14.0 (CH₃), 14.1 (CH₃), 20.3 (CH₂), 22.6 (CH₂), 27.0 (CH₂), 29.1 (CH₂), 30.0 (CH₂), 30.2 (CH₂), 31.9 (CH₂), 40.7 (CH₂), 46.4 (CH₂), 165.1 (C), 116.1 (C). Anal. Calcd for C₂₅H₅₀N₆·0.5H₂O: C, 67.67; H, 11.58; N, 18.94. Found: C, 67.53; H, 11.60; N, 18.32.

5,5-Diethyl-1-propyl-1,3-diazine-2,4,6(1H,3H,5H)-trione[56] **(4a).** A solution of **2a** (2 g, 10.9 mmol) and LiOH·H₂O (456 mg, 10.9 mmol) in formamide (16 mL) was stirred at 65 °C for 1 h. 1-Iodopropane (1.06 mL, 10.9 mmol) was then added, and stirring was continued at 100 °C for 19 h. The formamide was distilled off under vacuum to give a viscous oil that crystallized on shaking with H₂O (10 mL) to give pure **4a** (650 mg, 27%). An analytically pure sample was obtained
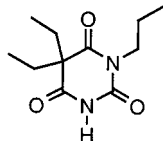

by recrystallization from CHCl₃/hexane to give colorless needles. Mp 109−110 °C; MS (FAB) *m/z* 227.2 (M + H); ^{1}H NMR (250 MHz, CDCl₃) δ 0.83 (t, *J* = 7.3 Hz, 6H), 0.95 (t, *J* = 7.3 Hz, 3H), 1.55−1.66 (m, 2H), 2.01 (q, *J* = 7.3 Hz, 4H), 3.86 (t, *J* = 7.6 Hz, 2H), 7.82 (br s, 1H); ^{13}C NMR (62.5 MHz, CDCl₃) δ 9.5 (CH₃), 11.2 (CH₃), 21.3 (CH₂), 32.7 (CH₂), 43.0 (CH₂), 58.3 (C), 149.8 (C), 171.8 (C), 172.3 (C). Anal. Calcd for C₁₁H₁₈N₂O₃: C, 58.39; H, 8.02; N, 12.38. Found: C, 58.46; H, 8.06; N, 12.37.

1,3-Bis(4′-isopropylphenyl)-1,3,5-triazine-2,4,6(1H,3H,5H)-tri-one[57] **(4b).** A solution of 4-(isopropyl)phenylisocyanate (1.01 g, 6.28 mmol) in DMF (2 mL) was added dropwise to a suspension of potassium cyanate (274 mg, 3.38 mmol) in DMF (4 mL) at 70 °C. The reaction was stirred for 1 h at 70 °C, and then for 20 h at 100 °C. The solvent was evaporated under reduced pressure, the residue shaken with H₂O (80 mL), and the resulting suspension filtered. The filtered residue was washed with H₂O (20 mL) and the filtrate treated with HCl (10 M) until a flocculent white precipitate had formed. Filtration and
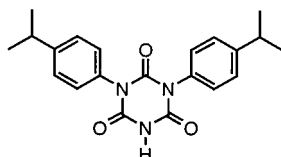
recrystallization of the filtered solid from chloroform−hexane gave **4b** as fine white crystals (624 mg, 54%). Mp 245−246 °C; MS (FAB) *m/z* 366.1 (M + H); ^{1}H NMR (250 MHz, CDCl₃) δ 1.25 (d, *J* = 7 Hz, 6H), 2.95 (m, 2H), 7.20−7.23 (m, 4H), 7.31−7.35 (m, 4H), 8.49 (br s, 2H); ^{13}C NMR (62.5 MHz, CDCl₃) δ 23.9 (CH₃), 33.9 (CH), 127.5 (CH), 128.1 (CH), 130.5 (C), 147.9 (C), 149.6 (C), 150.2 (C). Anal. Calcd for C₂₁H₂₃N₃O₃·0.5H₂O: C, 67.36; H, 6.46; N, 11.23. Found: C, 67.78; H, 6.11; N, 11.38.

1:1 Assembly 3f·4b. Addition of hexane to an equimolar solution of **3f** and **4b** in CH₂Cl₂ gave fine colorless needles. Integral values in
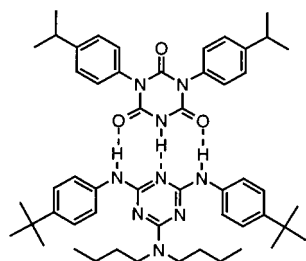
the ^{1}H NMR spectrum (CDCl₃) indicated that a 1:1 complex had

precipitated. Anal. Calcd for C₂₁H₂₃N₃O₃·C₃₁H₄₆N₆: C, 71.94; H, 8.01; N, 14.52. Found: C, 72.23; H, 8.00; N, 14.35.

1,3-N,N′-Bis[4-chloro-6-(tert-butylamino)-1,3,5-triazin-2-yl]xy-lylene Diamine (5a). A solution of 4-tert-butylaniline (0.52 g, 3.48 mmol) in THF (5 mL) was added to an ice-cooled solution of cyanuric chloride (0.63 g, 3.41 mmol) and DIPEA (2 mL) in THF (10 mL). The reaction was stirred for 1 h and allowed to warm to room temperature, and *m*-xylylene diamine (0.22 mL, 1.67 mmol) was added. Stirring was continued at 30 °C for 16 h, H₂O (80 mL) was added, and the oily suspension was shaken until the oil crystallized. The filtered
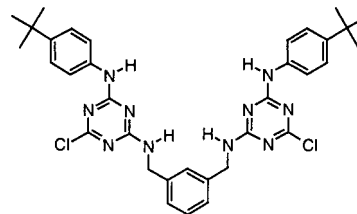

solid was recrystallized from a small quantity of CHCl₃ to give **5a** as a fine white powder (592 mg, 54%). MS (FAB) *m/z* 657.3 (M + H); ^{1}H NMR (250 MHz, CDCl₃) δ 1.29 (s, 18H), 4.60−4.68 (m, 4H), 7.21−7.40 (m, 14H), 8.32 (br s, 2H).

1,3-N,N′-Bis[4-(dibutylamino)-6-(tert-butylamino)-1,3,5-triazin-2-yl]xylylene Diamine (5b). A solution of **5a** (592 mg, 0.90 mmol) and dibutylamine (2 mL) in THF (10 mL) was refluxed for 3 d. The solvent was then evaporated under reduced pressure, and the residue was dissolved in CHCl₃ (100 mL), washed with H₂O (2 × 25 mL) and brine (25 mL), and dried on MgSO₄. Evaporation of the solvent under reduced pressure gave crude **5b** as a pale brown oil, which was purified
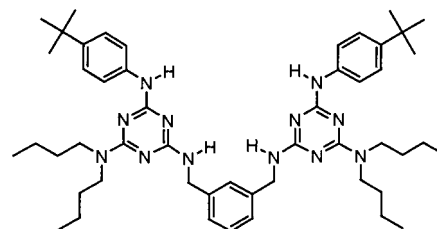
by column chromatography (SiO₂; EtOAc) to give **5b** as a colorless foam (697 mg, 97%). MS (FAB) *m/z* 843.7 (M + H); ^{1}H NMR (250 MHz, CDCl₃) δ 0.87−0.99 (m, 12H), 1.26−1.38 (m, 8H), 1.35 (s, 18H), 1.52−1.62 (m, 8H), 3.48 (m, 8H), 4.55 (d, *J* = 5.8 Hz, 4H), 5.30 (br s, 2H), 6.81 (br s, 2H), 7.22−7.28 (m, 8H), 7.48−7.51 (m, 4H); ^{13}C NMR (62.5 MHz, CDCl₃) δ 14.1 (CH₃), 20.3 (CH₂), 20.5 (CH₂), 30.2 (CH₂), 31.5 (CH₃), 34.2 (C), 44.4 (CH₂), 46.8 (CH₂), 47.2 (CH₂), 119.5 (CH), 125.3 (CH), 126.1 (CH), 128.6 (CH), 137.3 (C), 140.1 (C), 144.7 (C), 164.2 (C), 165.0 (C), 165.9 (C). Anal. Calcd for C₅₀H₇₄N₁₂: C, 71.22; H, 8.85; N, 19.94. Found: C, 71.19; H, 8.90; N, 19.98.

1:1 Assembly of 5b·2b. Et₂O was added dropwise to an equimolar solution of **5b** and **2b** in CH₂Cl₂. The resulting fine white solid was
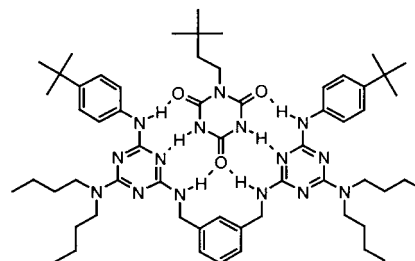

filtered and submitted for analysis. Mp 264−265 °C; ^{1}H NMR (250 MHz, CDCl₃) δ 0.96−1.01 (m, 21H), 1.18−1.44 (m, 26H), 1.54−1.66

(56) Chiron-Charrier, M.; Caubère, P. *Synth. Commun.* **1993**, *23*, 2659−2672.

(57) Argabright, P. A.; Williams, B. L. *J. Heterocycl. Chem.* **1970**, *7*, 725−728.

(m, 10H), 3.44−3.66 (m, 8H), 3.87−3.93 (m, 2H), 4.53−4.55 (m, 4H), 7.23−7.30 (m, 8H), 7.49 (br s, 2H), 7.68−7.75 (m, 4H), 9.53 (br s, 2H), 14.85 (br s, 2H); ^{13}C NMR (62.5 MHz, CDCl$_3$) δ 14.1 (CH$_3$), 20.3 (CH$_2$), 20.5 (CH$_2$), 29.2 (CH$_3$, isocyanurate), 30.0 (C, isocyanurate), 30.2 (CH$_2$), 31.5 (CH$_3$), 34.2 (C), 38.2 (CH$_2$, isocyanurate), 46.2 (CH$_2$), 47.1 (CH$_2$), 47.7 (CH$_2$), 119.8 (CH), 125.1 (CH), 127.9 (CH), 128.6 (CH), 137.5 (C), 137.8 (C), 144.8 (C), 153.3 (C=O, isocyanurate), 154.7 (C=O, isocyanurate), 161.6 (C), 162.9 (C), 164.1 (C), one aryl CH signal not observed. Anal. Calcd for C$_{50}$H$_{74}$N$_{12}$·C$_9$H$_{15}$N$_3$O$_3$·0.5H$_2$O: C, 66.51; H, 8.52; N, 19.72. Found: C, 66.63; H, 8.40; N, 19.40.

1:1 Assembly of 5b·2a. Addition of 95% EtOH to an equimolar solution of **5b** and **2a** in CH$_2$Cl$_2$ followed by evaporation of the CH$_2$-
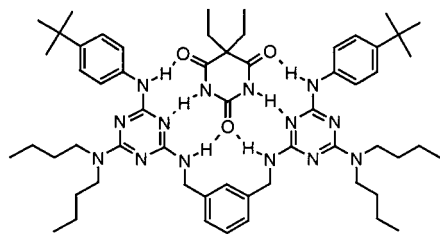
Cl$_2$ gave a fine white precipitate of the 1:1 complex. Mp 189−190 °C; ^{1}H NMR (250 MHz, CDCl$_3$) δ 0.90 (t, J = 7.3 Hz, 6H), 0.87−1.02 (m, 12H), 1.32 (s, 18H), 1.32−1.46 (m, 8H), 1.49−1.66 (m, 8H), 2.08 (q, J = 7.3 Hz, 4H), 3.52−3.66 (m, 8H), 4.57 (d, J = 4.0 Hz), 6.78 (br s, 2H), 7.26−7.32 (m, 8H), 7.70−7.74 (m, 4H), 9.07 (br s, 2H), 14.18 (br s, 2H); ^{13}C NMR (62.5 MHz, CDCl$_3$) δ 9.7 (CH$_3$, barbiturate), 14.1 (CH$_3$), 20.3 (CH$_2$), 20.5 (CH$_2$), 30.2 (CH$_2$), 30.2 (CH$_2$), 31.5 (CH$_3$), 32.2 (CH$_2$, barbiturate), 34.2 (C), 46.2 (CH$_2$), 46.9 (CH$_2$), 47.5 (CH$_2$), 57.7 (C, barbiturate), 119.8 (CH), 125.2 (CH), 128.0 (CH), 128.7 (CH), 129.8 (CH), 137.8 (C), 138.3 (C), 144.6 (C), 153.7 (C=O, barbiturate), 163.4 (C), 164.4 (C), 164.5 (C), 176.2 (C=O, barbiturate). Anal. Calcd

for C$_{50}$H$_{74}$N$_{12}$·C$_8$H$_{12}$N$_2$O$_3$·H$_2$O: C, 66.63; H, 8.29; N, 18.76. Found: C, 66.75; H, 8.41; N, 18.95.

Model Calculations. The models described in this paper (models 1 and 2) have been implemented in MicroMath Scientist 2.01 or Microsoft Excel 97. The experimentally determined K_0 and K_r values were used as input to calculate the fraction of free components **1** and **2**, rosette [**1**$_3$·**2**$_3$], and tapes [**1**·**2**]$_n$ in equilibrating the mixture of **1** and **2** under various conditions.

Molecular Mechanics Calculations. Initial structures as well as visualizations were generated using Quanta 97.[58] All gas-phase simulations were performed with CHARMm version 24.0[59−61] as implemented in Quanta 97. Parameters were taken from Quanta 97, and point charges were assigned with the charge template option. Residual charge was smoothed on carbon and nonpolar hydrogen atoms, rendering overall neutral residues. A distance-dependent dielectric constant was applied with ϵ = 1. No cutoffs on the nonbonded interactions were used. Energy minimizations were performed with the steepest descent and adopted basis Newton−Raphson methods until the root-mean-square of the energy gradient was <0.001 kcal mol^{-1} Å^{-1}.

(58) Quanta 97, Molecular Simulations, Waltham, MA.
(59) Brooks, B. R.; Bruccoleri, R. E.; Olafson, B. D.; States, D. J.; Swaminathan, S.; Karplus, M. *J. Comput. Chem.* **1983**, *4*, 187−217.
(60) Momany, F. A.; Klimkowski, V. J.; Schäfer, L. *J. Comput. Chem.* **1990**, *11*, 654−662.
(61) Momany, F. A.; Rone, R.; Kunz, H.; Frey, R. F.; Newton, S. Q.; Schäfer, L. *J. Mol. Struct. (THEOCHEM)* **1993**, *105*, 1−18.
(62) Chang, S.-K.; Hamilton, A. D. *J. Am. Chem. Soc.* **1988**, *110*, 1318−1319.